DIFFERENTIATION AND LOCALIZATION USING INFRARED SENSORS

A THESIS

SUBMITTED TO THE DEPARTMENT OF ELECTRICAL AND

ELECTRONICS ENGINEERING

AND THE INSTITUTE OF ENGINEERING AND SCIENCE

OF BİLKENT UNIVERSITY

IN PARTIAL FULFILLMENT OF THE REQUIREMENTS

FOR THE DEGREE OF

MASTER OF SCIENCE

By

Tayfun Aytaç

August 2002

I certify that I have read this thesis and that in my opinion it is fully adequate, in scope and in quality, as a thesis for the degree of Master of Science.

Assoc. Prof. Dr. Billur Barshan (Supervisor)

I certify that I have read this thesis and that in my opinion it is fully adequate, in scope and in quality, as a thesis for the degree of Master of Science.

Prof. Dr. Ömer Morgül

I certify that I have read this thesis and that in my opinion it is fully adequate, in scope and in quality, as a thesis for the degree of Master of Science.

Prof. Dr. Enis Çetin

Approved for the Institute of Engineering and Science:

Prof. Dr. Mehmet B. Baray
Director of the Institute Engineering and Science

ABSTRACT

DIFFERENTIATION AND LOCALIZATION USING INFRARED SENSORS

Tayfun Aytaç
M.S. in Electrical and Electronics Engineering
Supervisor: Assoc. Prof. Dr. Billur Barshan
August 2002

In this thesis, different approaches for the differentiation and localization of targets using low-cost infrared sensors are presented. The intensity readings obtained with such sensors are highly dependent on the location and properties of targets in a way which cannot be represented in a simple manner, making the differentiation and localization process difficult. We propose the use of angular intensity scans and present different approaches to process them. Using these approaches, targets of different geometrical shapes but identical surface properties, targets of different surface properties but identical geometry, and targets having both different geometrical shapes and surface properties are differentiated and localized in a position-invariant manner. Maximum correct differentiation rates of 97%, 87%, and 65% are respectively achieved in these cases, indicating that the geometrical properties of targets are more distinctive than their surface properties in the differentiation process. The different approaches are verified experimentally with target types of commonly encountered geometries in indoor environments and with surfaces of different reflection properties. The results indicate that simple infrared sensors, when coupled with appropriate processing, can be used to extract a significantly greater amount of information than they are commonly employed for.

Keywords: pattern recognition and feature extraction, infrared sensors, target differentiation and localization, surface recognition, position estimation.

ÖZET

KIZILÖTESİ ALGILAYICILAR İLE AYIRDETME VE KONUMLANDIRMA

Tayfun Aytaç
Elektrik ve Elektronik Mühendisliği, Yüksek Lisans
Tez Yöneticisi: Doç. Dr. Billur Barshan
Ağustos 2002

Bu tezde, düşük maliyetli kızılötesi algılayıcıların ayırdetme ve konumlandırma amacıyla kullanımı için farklı yaklaşımlar sunulmuştur. Bu tip algılayıcılardan elde edilen yeğinlik ölçümleri büyük ölçüde hedefin konumuna ve özelliklerine bağlı olup, bu ilişki analitik olarak kolayca ifade edilememektedir. Bu çalışmada açısal yeğinlik taramalarının kullanımını ileri sürüyor ve onları işleyen yaklaşımlar sunuyoruz. Bu yaklaşımlar kullanılarak benzer geometrik şekillere fakat farklı yüzey özelliklerine sahip hedefler, benzer yüzey özelliklerine fakat farklı geometrik şekillere sahip hedefler ve hem farklı yüzey hem de farklı geometrik şekle sahip hedefler konumdan bağımsız olarak ayırdedilmiş ve konumlandırılmıştır. Bu durumlarda en büyük doğru ayırdetme oranları, ayırdetme sürecinde hedeflerin geometrik özelliklerinin yüzey özelliklerinden daha ayırdedici olduğunu gösterir şekilde, sırasıyla %97, %87 ve %65 olarak elde edilmiştir. Farklı yaklaşımlar deneysel olarak kapalı mekanlarda sıkça karşılaşılan geometrilere sahip hedeflerle ve farklı yansıma özelliklerine sahip yüzeylerle değerlendirilmiştir. Sonuçlar, basit kızılötesi algılayıcıların uygun işleme yöntemleri kullanıldığı takdirde yaygın uygulamalarındakine göre çok daha fazla bilgi çıkarımında kullanılabileceğini göstermektedirler.

Anahtar sözcükler: örüntü tanıma ve öznitelik çıkarımı, kızılötesi algılayıcılar, hedef ayırdetme ve konumlandırma, yüzey tanıma, pozisyon kestirimi.

Acknowledgment

I would like to express my gratitude to my supervisor Assoc. Prof. Dr. Billur Barshan for her guidance, support, and encouragement throughout the development of this thesis.

I would like to express my special thanks and gratitude to Prof. Dr. Ömer Morgül and Prof. Dr. Enis Çetin for showing keen interest in the subject matter and accepting to read and review the thesis.

Contents

List of Figures

List of Tables

Chapter 1

INTRODUCTION

Differentiation and localization is of considerable interest for intelligent systems where there is need to identify objects and their positions for autonomous operation. A mobile robot must interact with its environment and identify objects to accomplish its tasks efficiently. Differentiation is also important in industrial applications where different materials must be identified and separated. In this thesis, we consider the use of a simple infrared sensing system consisting of one emitter and one detector for these purposes.

Infrared sensors are inexpensive, practical, and widely available. The emitted light is reflected from the target and its intensity is measured at the detector. However, it is often not possible to make reliable distance estimates based on the value of a single intensity return because the return depends on both the geometry and other properties of the reflecting target. Likewise, the properties of the target cannot be deduced from simple intensity returns without knowing its distance and angular location.

Most work on pattern recognition involving infrared deals with recognition or detection of features or targets in conventional two-dimensional images. Examples of work in this category include face identification [1], automatic target recognition [2], target tracking [3], automatic vehicle detection [4], remote sensing [5], detection and identification of targets in background clutter [6, 7],

and automated terrain analysis [8]. We note that the position-invariant pattern recognition and position estimation achieved in this thesis is different from such operations performed on conventional images [9, 10] in that here we work not on direct "photographic" images of the targets obtained by some kind of imaging system, but rather on angular intensity scans obtained by rotating a point sensor. The targets we differentiate are not patterns in a two-dimensional image whose coordinates we try to determine, but rather objects in space, exhibiting depth, whose position with respect to the sensing system we need to estimate. As such, position-invariant differentiation and localization is achieved with an approach quite different than those employed in invariant pattern recognition and localization in conventional images [11–18].

Application areas of infrared sensing include robotics and automation, process control, remote sensing, and safety and security systems. More specifically, infrared sensors have been used in simple object and proximity detection, counting [19, 20], distance and depth monitoring [21], floor sensing, position control [22], obstacle/collision avoidance, and machine vision systems [23]. Infrared sensors are used in door detection [24], mapping of openings in walls [25], as well as monitoring doors/windows of buildings and vehicles, and "light curtains" for protecting an area. In [26], an automated guided vehicle detects unknown obstacles by means of an "electronic stick" consisting of infrared sensors, using a strategy similar to that adopted by a blind person. In [27], infrared sensors are employed to locate edges of doorways in a complementary manner with sonar sensors. Other researchers have also dealt with the fusion of information from infrared and sonar sensors [28, 29] and infrared and radar systems [30, 31]. In [32], infrared proximity sensing for a robot arm is discussed. Following this work, [33] describes a robot arm completely covered with an infrared skin sensor to detect nearby objects. In another study [34], the properties of a planar surface at a known distance have been determined using the Phong illumination model [35], and using this information, the infrared sensor employed has been modeled as an accurate range finder for surfaces at short ranges. Reference [36] also deals with determining the range of a planar surface. By incorporating the optimal amount of additive noise in the infrared range measurement system, the authors were able

to improve the system sensitivity and extend the operating range of the system. A number of commercially available infrared sensors are evaluated in [37] for space applications. References [38, 39] describe a passive infrared sensing system which identifies the locations of the people in a room. Infrared sensors have also been used for automated sorting of waste objects made of different materials [40, 41]. However, to the best of our knowledge, no attempt has been made to differentiate and estimate the position of targets of different geometries and surface properties using infrared sensors.

The main contribution of this thesis is that, even though the intensity patterns are highly dependent on target location and properties, and this dependence cannot be represented by a simple relationship, we achieve position-invariant differentiation and localization of targets of different geometries and surface properties. The results indicate that geometrical properties of targets are much more distinctive than their surface properties in the differentiation process. Our results show that it is possible to extract a significantly greater amount of information from simple optical sensors than they are commonly employed for (e.g., the emitter and detector pair employed in this thesis is marketed as a simple proximity switch).

The thesis is organized as follows: Chapter 2 gives a brief account of basics of infrared sensing and investigates infrared sensors in terms of parameters affecting their operation. Chapter 3 introduces a rule-based algorithm to differentiate and localize commonly encountered target primitives in indoor environments of different geometries, such as planes, corners, edges, and cylinders using two infrared sensors. In Chapter 4, template-based differentiation and localization is achieved using a single infrared sensor. Algorithms are verified both for targets of different geometries and surfaces of different reflection properties. Chapter 5 deals with the simultaneous deduction of not only the geometry but also the surface properties of the targets using a similar approach. Finally, in Chapter 6, results are discussed and directions for future research are provided. Sample codes for the programs written are provided in the disk.

Chapter 2

INFRARED SENSING

Infrared sensors are inexpensive, practical, and widely available devices. They can be classified according to their emitter-detector configuration into four groups as opposed, retroreflective, diffuse, and convergent modes [23] (Figure 2.1). Opposed mode is used, for instance, in remote controls. The retroreflective mode, in which the emitted energy is reflected from a retroreflector, such as a corner cube is commonly used in, for instance, doorway detectors in buildings. It is also used for reference marking purposes in automated guided vehicles. Mostly used in object detection is the diffuse mode, where the emitted energy is reflected from the object of interest. In the convergent mode, the optical axis of the emitter-detector is tilted in order to detect objects over a specific range.

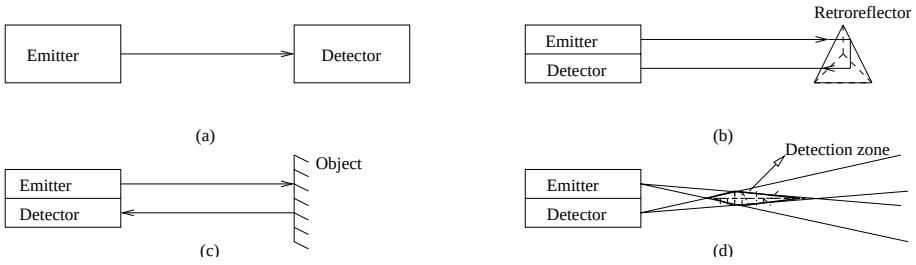

Figure 2.1: (a) Opposed, (b) retroreflective, (c) diffuse, and (d) convergent modes.

The operation of the infrared sensor used in this thesis depends on range estimates based on the return signal intensity. As the distance increases, the return

signal intensity decreases. In our experimental work, the IRS-U-4A infrared sensor [42] is used. The sensor works with 20–28 V DC input voltage, and provides an analog output voltage proportional to the measured intensity. The detector window is covered with an infrared filter to minimize the effect of ambient light on the intensity measurements. Indeed, when the emitter is turned off, the detector reading is essentially zero. The constant factor multiplying the nonlinear relationship between the range and the output intensity can be adjusted with a potentiometer, thus determining the range of operation of the system with the present device.

We believe that for proper operation of a sensor, the parameters affecting its operation should be thoroughly investigated. In this section, the effects of parameters such as range, azimuth, and surface properties of planar surfaces on the operation of the sensor are investigated. Various surfaces with different

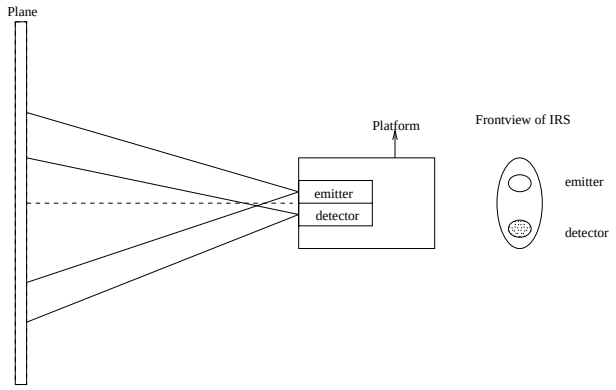

Figure 2.2: Experimental setup to analyze the effect of various parameters on the performance of the infrared sensor.

colors and surface properties have been considered. To analyze the effect of the surface roughness, packing materials with different reflection properties are employed. The experimental setup used for this purpose is shown in Figure 2.2, where a planar surface is employed for the purpose of uniform characterization of different surfaces. The plane is chosen large enough to contain the infrared spot size. The optical axis of the infrared sensor is coincident with the normal of the plane. Measurements are taken with the potentiometer adjusted both at its rightmost and leftmost positions, corresponding to minimum and maximum

range of operation, respectively.

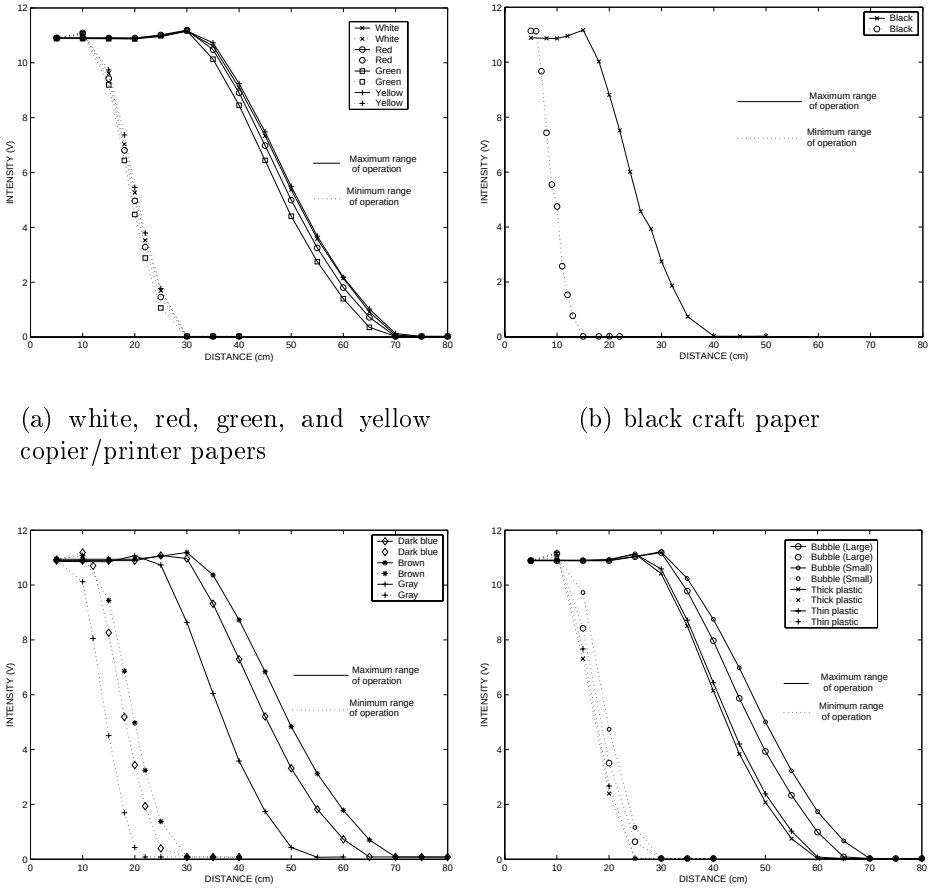

(a) white, red, green, and yellow copier/printer papers

(b) black craft paper

(c) drawing papers of different colors

(d) various packing materials

Figure 2.3: Intensity versus distance characteristics for planar targets of different surface properties.

To study the effect of target range, azimuth, and surface parameters on the measurements, intensity samples are acquired for each position and surface, and their mean and standard deviations are calculated. In Figure 2.3(a), the plots of intensity versus distance are given for the plane covered with white, red, green, and yellow copier/printer papers. Notice that for each color, there is a certain range of operation determined by saturation at the lower end and loss of signal at the higher end (beyond a certain range, the output voltage is not detectable). For the situation where the potentiometer is adjusted at its rightmost position,

it is possible to deduce the range of the plane of different colors within a few centimeter error. We observe that the color does not have a strong effect on the output intensity which makes the system suitable for range detection of different colored surfaces.

Unlike the planes above, the plane covered with glossy, smooth, black plane (craft paper) showed different behavior due to its high absorption property (Figure 2.3(b)).

Drawing papers having gray, dark blue, and brown colors are also employed. These papers are slightly thicker than copier papers and have a little more roughness on one side than the other. Because of their different surface properties, their characteristics differ from those of the copier papers. The intensity variations with respect to distance are given in Figure 2.3(c).

Blister packaging materials made of transparent colorless nylon with large and small bubbles and styrofoam packaging materials are also used to investigate the effect of different surface properties on the measurements. The blister packaging material with small bubbles has a honeycomb pattern of uniformly distributed circular bubbles of diameter 1.0 cm and height 0.3 cm, with a center-to-center separation of 1.2 cm. The blister packaging material with large bubbles has the same pattern with diameter, height, and center-to-center separation of 2.5 cm, 1.0 cm, and 2.8 cm, respectively. The variation of the intensity with respect to distance is given in Figure 2.3(d). The styrofoam packaging material absorbs more energy than the blister packaging materials. As expected, for a given distance, the return signal for the plane with small bubbles is greater than that with large bubbles. This is the result of enhanced multi-directional reflection due to large bubbles.

In Figure 2.4, the results obtained with both sides of the gray drawing paper are displayed, one surface being slightly rougher than the other. As seen from the graph, the surface roughness may result in erroneous readings even for a plane of the same color.

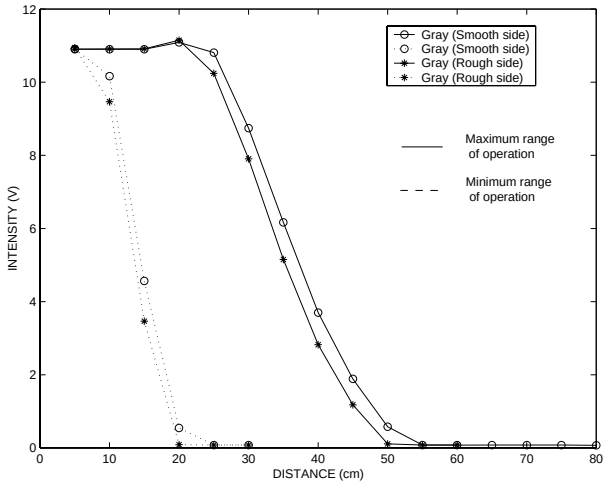

Figure 2.4: Effect of surface roughness on the intensity readings for a plane of gray drawing paper.

The variation of the standard deviation with respect to distance for various planes is given in Figure 2.5. For a given distance value and a surface type, the standard deviation was calculated over 10,000 intensity measurements. The standard deviation varies approximately within a band of 0.04 $\pm$0.01 V.

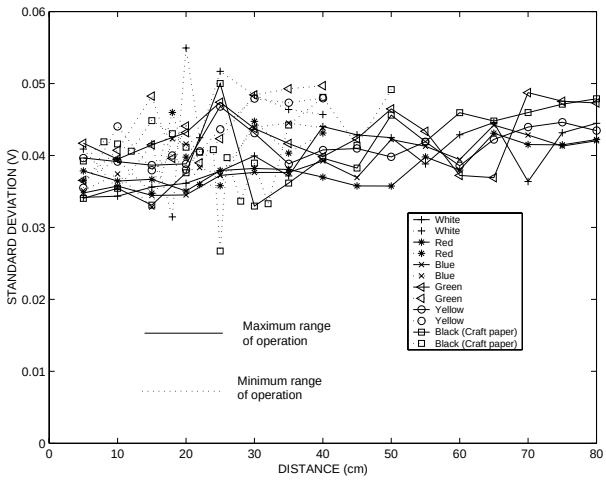

Figure 2.5: Standard deviation versus distance characteristics for various planes.

The variation of the standard deviation with respect to the scan angle is illustrated in Figure 2.6 for a wooden plane located at r =35 cm and $\theta = 0^\circ$. The

mean and the standard deviation values of the scan were calculated over 1,000 intensity measurements at each step of the scan. Figure 2.6 illustrates the mean value $\pm 25\sigma$. The standard deviation was calculated to vary between a minimum value of 0.006 V and a maximum value of 0.04 V.

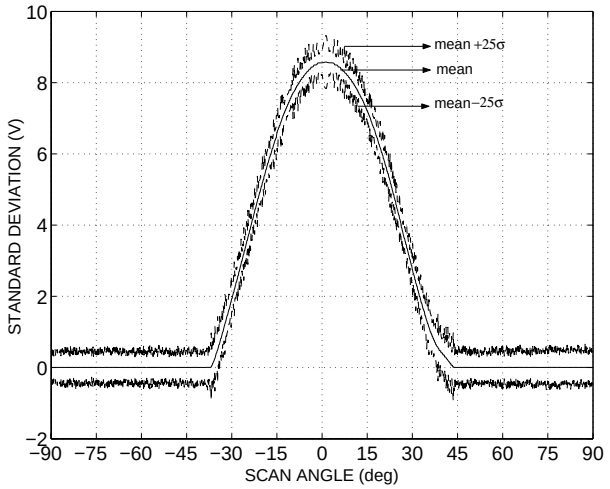

Figure 2.6: The mean and the $\pm 25\sigma$ of the intensity measurements versus scan angle for a wooden plane located at r =35 cm and $\theta = 0°$.

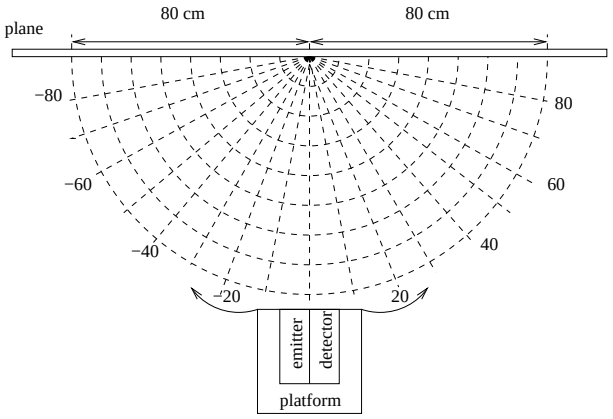

Figure 2.7: Experimental setup to observe the detectable range of a planar surface.

Now, we turn our attention to the problem of determining the operating range and angle of our system. To this end, the sensing unit will be situated on the grid points shown in Figure 2.7, in each case pointing towards the center of the radial

grid. We have considered both extreme settings of the potentiometer. Using the plane covered with white copier/printer paper, measurements are taken at 5 cm intervals from 5 cm to 80 cm, and at $\theta = 10^\circ$ intervals from $\theta = 0^\circ$ and $\theta = 80^\circ$ with the normal of the plane (smooth, white plane is chosen to minimize the effect of the diffuse reflectance ratios [43]).

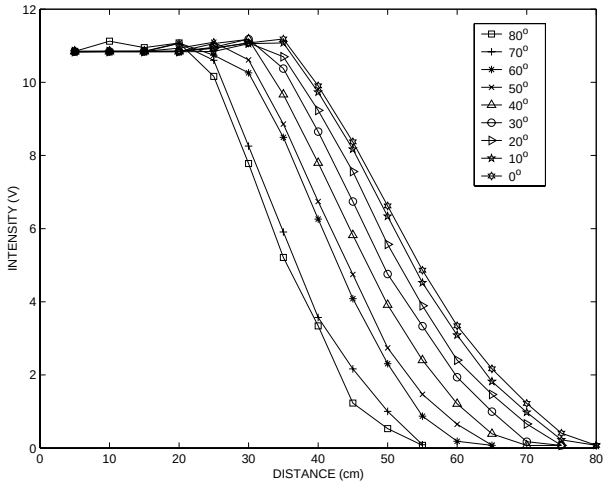

Figure 2.8: Variation of the intensity with respect to distance and angle for a smooth, white plane.

The variation of the intensity with respect to distance and angle for the white plane is given in Figure 2.8. By using these plots, the detectable range of the plane is given in Figure 2.9. The outer curve is composed of points whose intensities are less than 0.1 V, and the inner curve is composed of points whose intensities are greater than or equal to 0.1 V. The curves are given both for the rightmost (solid lines) and leftmost (dashed lines) positions of the potentiometer. For the rightmost position of the potentiometer, the infrared sensor can detect the plane making $\theta = 80^\circ$ angle with the normal of the plane at 50 cm. On the other hand, at the same angle, the infrared sensor can detect the plane at 20 cm at the leftmost position of the potentiometer. As seen from the plot, the intensity depends on the position of the plane with respect to the infrared sensor. As the line-of-sight of the infrared sensor deviates from the normal of the plane, the intensity decreases (Figure 2.8).

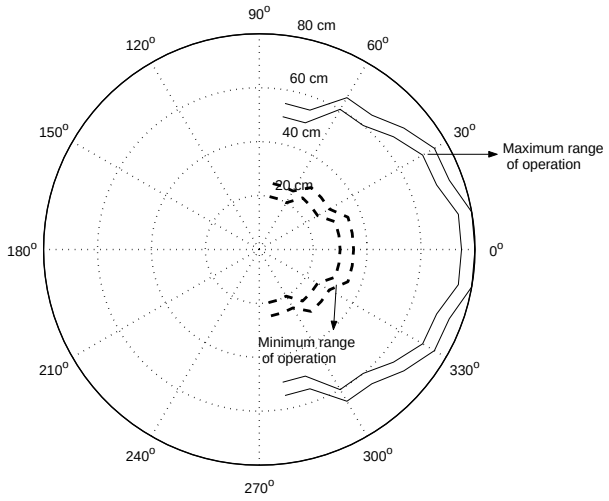

Figure 2.9: Detectable range of a smooth white plane by the infrared sensors.

Light reflected from objects depends on the intensity, wavelength, and distance of the incident light, the properties of the light source (i.e., point or diffuse source) and the surface properties of the objects under consideration such as reflectivity, absorbtivity, and the orientation [43, 44].

Matte materials can be approximated as ideal Lambertian surfaces which absorb no light and reflect all incident light with equal intensities in all directions with respect to the incidence angle [43, 45, 46]. When a Lambertian surface is illuminated by a point source of irradiance E, then the reflection function will be

$$\mathcal{I} = \frac{1}{\pi} E \cos(\theta_i), \quad \text{for} \quad \theta_i \geq 0, \tag{2.1}$$

which is known as "cosine" or Lambert's law of reflection from matte surfaces.

Perfect reflectors reflect all incident light in the plane defined by the incident light and the surface normal, making an angle of θ_e with the surface normal, which is equal to the incidence angle θ_i.

Many surfaces are modeled as Lambertian with additional specular-reflection component (Figure 2.10). According to the Phong illumination model [35], reflectance is given by

$$\mathcal{R} = R_2 \cos(\theta_i) + R_1(\theta_i) \cos(\theta_s)^n + R_0 \tag{2.2}$$

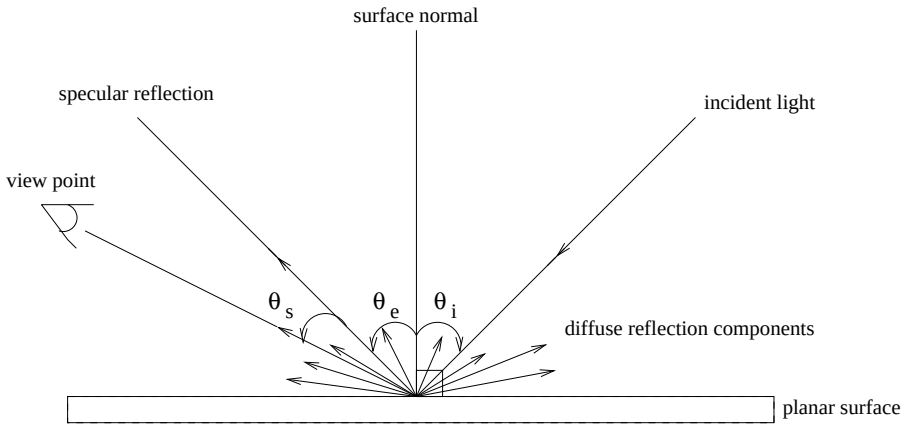

Figure 2.10: Model of reflection from an opaque surface.

where R_2 and R_0 are constants due to the reflection coefficient of the surface and environmental diffuse reflection coefficient, n models the specular reflected light for each material, and $R_1(\theta_i)$ gives the ratio of the reflected light and the incident light in terms of the incidence angle θ_i. In [34], this simple nonemprical mathematical model is used to model reflections from planar surfaces by fitting the reflectance data to the model in Equation (2.2).

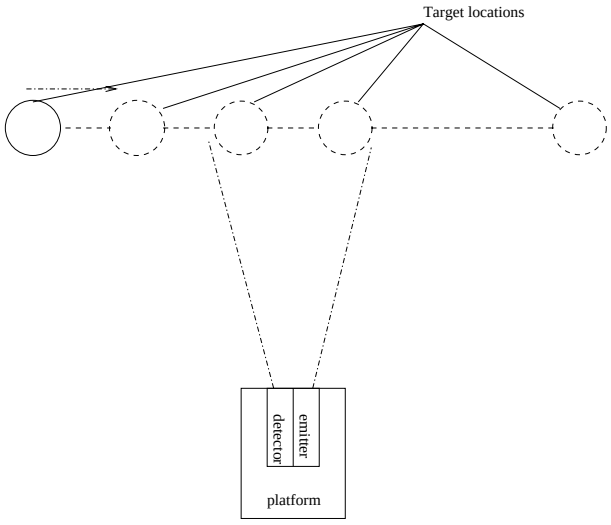

Figure 2.11: Experimental setup for the estimation of the beamwidth of the infrared sensor.

Because infrared sensors function similarly to radar sensors except for using

optical energy rather than radio-frequency energy, the experimental estimation of the beamwidth is accomplished using the setup shown in Figure 2.11 [47]. The half-power beamwidth of the infrared sensor is found by setting the intensity to $1/\sqrt{2}$ of the maximum reading obtained. The half-power beamwidth is found to be approximately $\theta = 3.3^{\circ}$ (Figure 2.12), which makes it useful for object detection due to its acceptable angular resolution.

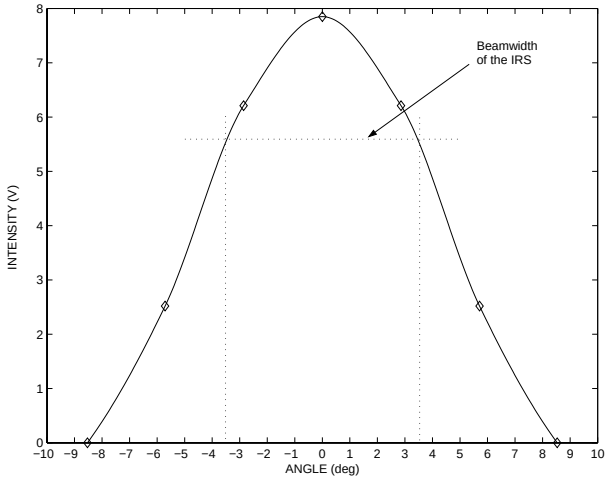

Figure 2.12: The half-power beamwidth of the infrared sensor.

In this chapter, a low-cost infrared sensor is evaluated in terms of the parameters affecting the return signal intensity such as the range, azimuth, and the surface parameters of the target. Based on these results we developed different approaches for target differentiation and localization in the following chapters.

Chapter 3

RULE-BASED TARGET DIFFERENTIATION AND LOCALIZATION

In this chapter, we propose a scanning mechanism and a rule-based algorithm which differentiates targets independent of their locations. The proposed method has the advantage that it does not require storage of any reference templates because the information necessary to differentiate the targets are completely embodied in a set of rules.

The target primitives employed in this study are plane, 90° corner, 90° edge, and a cylinder of radius 4.8 cm, whose cross-sections are illustrated in Figure 3.1. They are made of wood, each with a height of 120 cm. Our method is based on angularly scanning each target over a certain angular range.

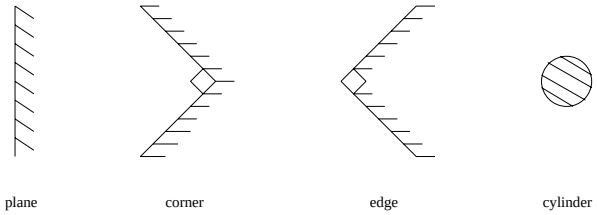

Figure 3.1: Target primitives used in the experiment.

We considered the use of two infrared sensors mounted on a 12 inch rotary table [48] horizontally, with a center-to-center separation of 11 cm (Figure 3.2). Targets are scanned from $-60°$ to $60°$ with $0.15°$ increments, and the mean of 100 samples are calculated at each position of the rotary table. The outputs of the infrared sensors are multiplexed to the input of a 8-bit microprocessor compatible A/D converter chip having a conversion time of 100 μsec.

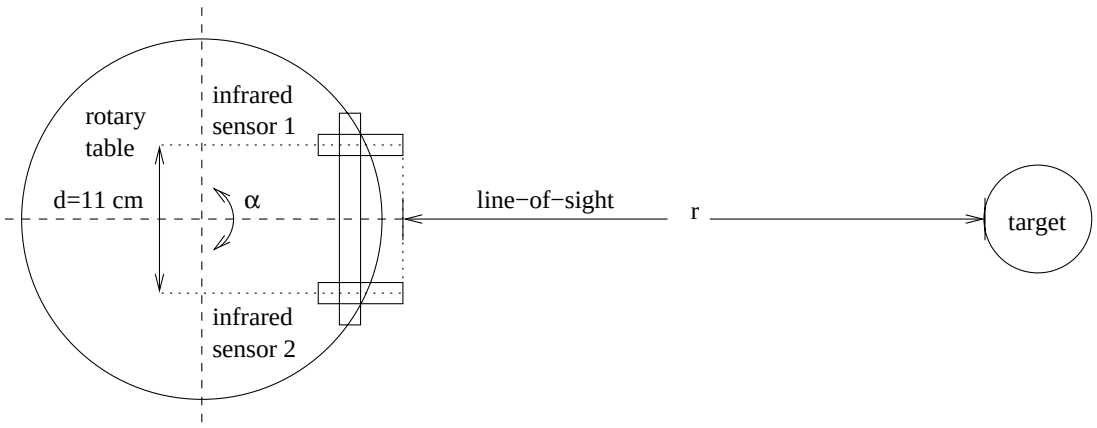

Figure 3.2: Top view of the experimental setup. Both the scan angle α and the target azimuth θ are measured counter-clockwise from the horizontal axis.

3.1 The Algorithm

Some sample scan patterns obtained from the targets are shown in Figure 3.3. Based on these patterns, it is observed that the return signal intensity patterns for a corner (Figure 3.3(b)), which have two maxima and a single minimum (a double-humped pattern), differ significantly from those of other targets which have a single maximum. The double-humped pattern is a result of the two orthogonal planes constituting the corner. Because of these distinctive characteristics, the corner differentiation rule is employed first. We check if the scan pattern has two humps or not. If so, it is a corner. The average of the angular locations of the dips in the middle of the two humps for the left and right infrared sensors provides an estimate of the angular location of the corner. As can be guessed, this distinctive signature can also be obtained using a single infrared sensor, but

the use of two infrared sensors becomes critical in the differentiation of planes, edges, and cylinders.

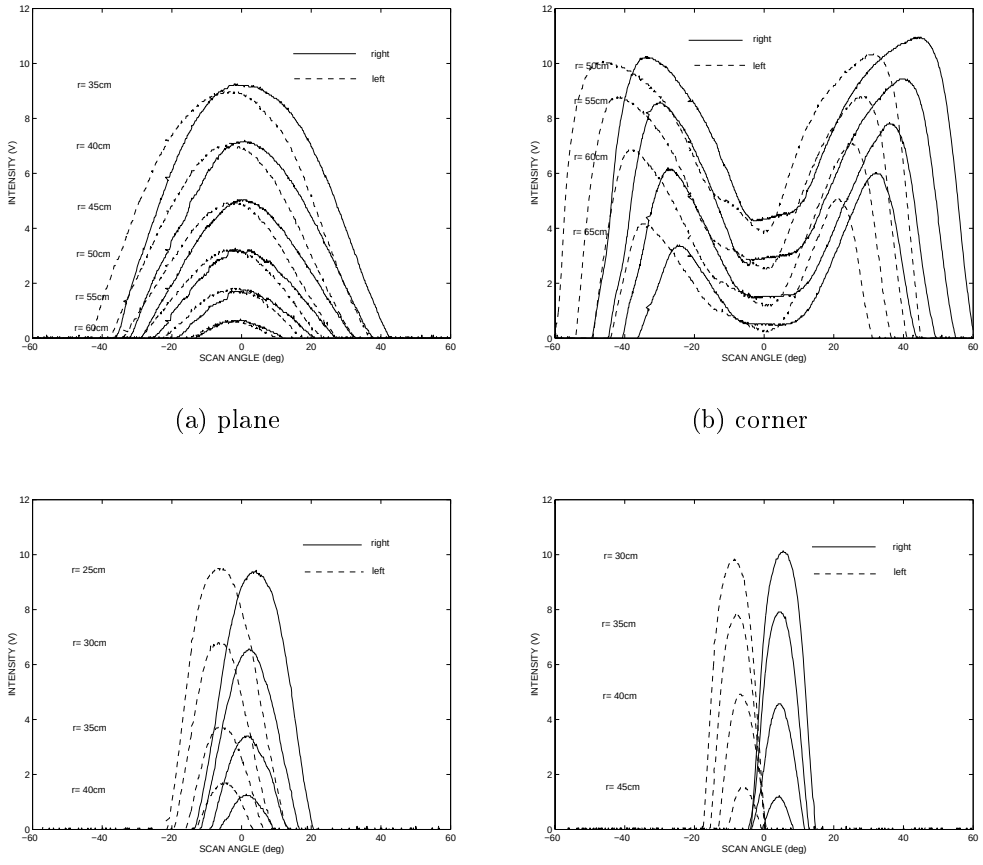

(a) plane

(b) corner

(c) edge

(d) cylinder

Figure 3.3: Intensity versus scan angle characteristics for various targets along the line-of-sight of the experimental setup.

If the target is found not to be a corner, we next check whether it is a plane or not. As seen in Figure 3.3(a), the difference between the angular locations of the maximum readings for planar targets is significantly smaller than that of other targets. Planar targets are differentiated from the remaining targets by comparing the absolute difference of the angle values at which the two intensity patterns have their maxima. (In the experiments, we have used a reference value of 6.75°.) The azimuth estimation of planar target is accomplished by averaging the angular locations of the maxima of the two return signal intensities.

Notice that the above (and following) rules are designed to be independent of those features of the scans which vary with range and azimuth so as to enable position-invariant recognition of the targets. In addition, the proposed method has the advantage that it does not require storage of any reference templates since the information necessary to differentiate the targets are completely embodied in the set of decision rules.

If the target is not a plane either, we next check whether it is an edge or a cylinder. The intensity patterns for the edge and cylinder targets are given in Figures 3.3(c) and (d). They have shapes similar to those of a planar target, but the intersection points of the intensity patterns differ significantly from those of planar targets. In the differentiation of edges and cylinders, the ratio of the intensity value at the intersection of the scans corresponding to the two infrared sensors, to the maximum intensity value of the pattern is employed. (Because the maximum intensity values of the right and left infrared sensors are very close, the maximum intensity reading of either infrared sensor or their average can be used in this computation.) This ratio is compared with the experimentally obtained reference values to determine whether the target is an edge or a cylinder. If the ratio is greater than the reference value, it is an edge, otherwise, a cylinder. (In our experiments, the reference value was 0.65.) If the scan patterns from the two sensors do not intersect, the algorithm cannot distinguish between cylinders and edges. However, this never occurred in our experiments. The azimuth estimate of edges and cylinders is also obtained by averaging the angular locations of the maxima of the two scans. Having determined the target type and estimated its azimuth, its range can also be estimated by using linear interpolation between the central values of the individual intensity scans given in Figure 3.3.

3.2 Experimental Verification

Using the experimental setup described in Section 2, the algorithm presented in the previous section is used to differentiate and estimate the position of a plane, 90° corner and 90° edge, and a cylinder of radius 4.8 cm.

Based on the results of 160 experimental test scans, the target confusion matrix shown in Table 3.1, which contains information about the actual and detected targets, is obtained. The average accuracy over all target types can be found by summing the correct decisions given along the diagonal of the confusion matrix and dividing this sum by the total number of test scans (160) resulting in an average accuracy of 91% over all target types. Targets are localized within absolute average range and azimuth errors of 0.55 cm and 1.03°, respectively. The percentage-wise accuracy for each target type and confusion rates are presented in Table 3.2. The second column of the table gives the percentage accuracy of correct differentiation of the target and the third column gives the percentage of cases when a certain target was mistaken for another. The fourth column gives the total percentage of other target types that were mistaken for a particular target type. For instance, for the planar target $(4+3)/43 = 16.3\%$, meaning that targets other than planes are incorrectly classified as planes with a rate of 16.3%.

Table 3.1: Target confusion matrix (P: plane, C: corner, E: edge, CY: cylinder).

target	differentiation result				total
	P	C	E	CY	
P	36	–	4	–	40
C	–	40	–	–	40
E	4	–	33	3	40
CY	3	–	–	37	40
total	43	40	37	40	160

Because the intensity pattern of a corner differs significantly from the rest of the targets, the algorithm differentiates corners accurately with a rate of 100%. A target is never classified as a corner if it is actually not a corner. Edges and cylinders are the most difficult targets to differentiate. It may be considered fortunate that edges and cylinders tend to be in general less common than planes and corners in typical indoor environments.

Table 3.2: Performance parameters of the algorithm (P: plane, C: corner, E: edge, CY: cylinder).

actual target	correct diff. rate (%)	differen. error I (%)	differen. error II (%)
P	90	10	16.3
C	100	0	0
E	82.5	17.5	10.8
CY	92.5	7.5	7.5
overall	91.25	8.75	8.65

3.3 Conclusion

In this chapter, rule-based differentiation and localization of commonly encountered targets such as planes, corners, edges, and cylinders is achieved using intensity measurements from inexpensive infrared sensors. We proposed a scanning mechanism and a rule-based algorithm based on two infrared sensors to differentiate targets independent of their positions. We have shown that the resulting angular intensity scans contain sufficient information to identify several different target types and estimate their range and azimuth. The rule-based algorithm is evaluated in terms of correct target differentiation rate, and range and azimuth estimation accuracy.

The accomplishment of this chapter is that even though the intensity scan patterns are highly dependent on target location, and this dependence cannot be represented by a simple relationship, we achieve position-invariant target differentiation using a rule-based differentiation algorithm. By designing the decision rules so that they do not depend on those features of the scans which vary with range and azimuth, an average correct target differentiation rate of 91% over all target types is achieved and targets are localized within average absolute range and azimuth errors of 0.55 cm and 1.03°, respectively. The proposed method has the advantage that it does not require storage of any reference templates because the information necessary to differentiate the targets are completely embodied in the set of rules.

Chapter 4

TEMPLATE-BASED DIFFERENTIATION AND LOCALIZATION

In this chapter, methods to differentiate and localize targets using a single infrared sensor are proposed, and different approaches are compared in terms of their correct differentiation rates, and range and azimuth estimation accuracies. Both targets of different geometries but fixed surface properties and targets of fixed geometries but variable surface properties are considered. The approach differs from that in Chapter 3 in the sense that it uses the intensity scans obtained with the infrared sensor as templates and reveals the distinctive features of the intensity scans by applying pattern recognition techniques.

4.1 Position-Invariant Target Differentiation and Localization

The targets employed are plane, 90° corner, 90° edge, and a cylinder of radius 4.8 cm, whose cross-sections were given in Figure 3.1. Our method is based on

angularly scanning each target over a certain angular range. The infrared sensor is mounted on a 12 inch rotary table [48] (Figure 4.1) to obtain angular scans from these target primitives. Reference data sets are collected for each target at $\theta = 0^\circ$ with 2.5 cm distance increments, ranging from 15 cm to the maximum detectable range of each target.

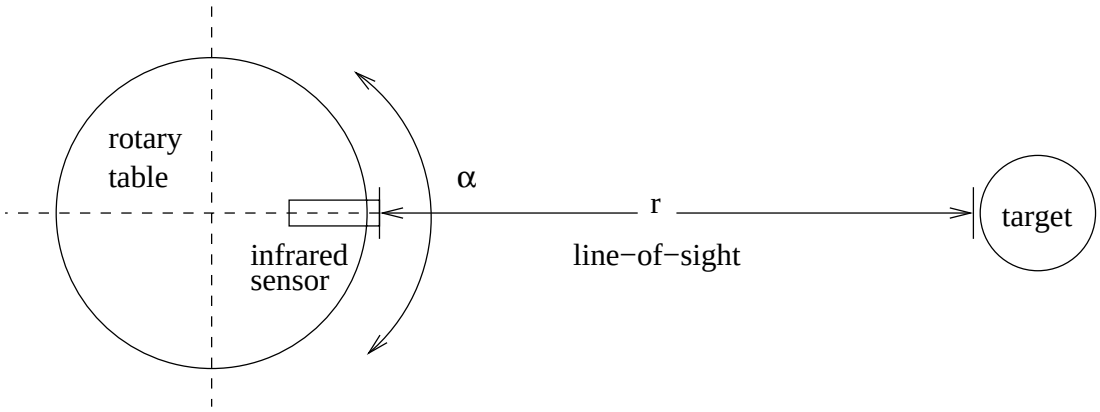

Figure 4.1: Top view of the experimental setup. The emitter and detector windows are circular with 8 mm diameter and center-to-center separation of 12 mm. (The emitter is above the detector.) Both the scan angle α and the target azimuth θ are measured counter-clockwise from the horizontal axis.

The resulting reference scans for plane, corner, edge, and cylinder are shown in Figures 4.2(a)–(d), respectively. The intensity scans are θ-invariant but not r-invariant; changes in r do not result in any simple scaling. As we will see, these scans contain sufficient information to identify and localize the different target types with a good degree of accuracy. Figure 4.2(b) shows the distinctive double-humped scan pattern for the corner target (this double-humped pattern can be interpreted by thinking of the corner in terms of its two orthogonal constituent planes). As can be guessed from these figures, the greatest difficulty is encountered in differentiating cylinders and edges which have the most similar intensity patterns. Notice that the return signal intensities saturate at an intensity corresponding to 10.7 V output voltage.

We now describe how to determine the target type and the position of an arbitrarily located target whose intensity scan has been observed. First, we check

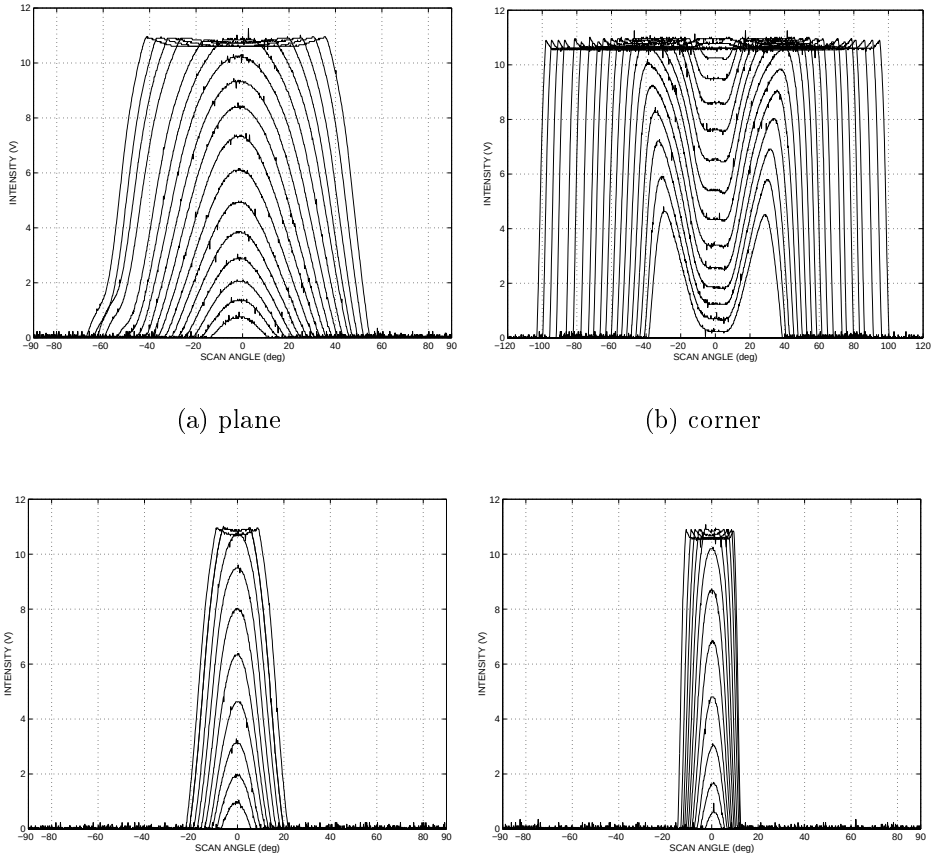

(a) plane (b) corner

(c) edge (d) cylinder

Figure 4.2: Intensity scans for targets at various distances.

whether the observed scan $I(\alpha)$ exhibits saturation or not. This situation is treated separately as will be explained later in Section 4.1.3. A corner scan is considered saturated when its central intensity enters the saturation region, not the humps, since it is the former value which is critical for our method below.

We start by determining the target type. Unfortunately, direct comparison with the corresponding curves in Figures 4.2(a)–(d) is not possible because we do not yet know the distance to the target, and comparing with all the curves at all distances would be computationally very expensive. Therefore, we exploit the fact that the successive curves in Figures 4.2(a)–(d) exhibit a monotonic dependence on distance. Furthermore, when an observed scan is compared to

the several successive curves in any of Figures 4.2(a)–(d), the two measures of difference between them described in Sections 4.1.1 and 4.1.2 below also exhibit a monotonic fall and rise around a single minimum. Therefore, we are assured that we will not be settling at a suboptimal point if we compare the observed scan not with all scans at all distances but only with the four scans (one for each target type) whose central intensities are closest to that of the observed scan. Therefore, for unsaturated scans, only four comparisons need to be made. This remains the case even if the 2.5 cm increments are reduced to smaller values. This has the advantage that the accuracy of the system can be increased without increasing the cost of computation (although a greater number of scans do have to be stored). As a test, we also ran a version of the method where *eight* comparisons were made using the scans with the nearest central intensities both above *and* below the observed central intensity, and also using *all* of the scans shown in Figures 4.2(a)–(d). These computationally more expensive approaches, exceedingly more so in the latter case, did not improve the result with respect to comparison with only four scans. In fact, in the matched filtering case discussed in Section 4.1.2, the results are even somewhat better when four scans are used, due to the fact that this systematic elimination of a priori suboptimal scans eliminates the small possibility that they will mistakenly be chosen as the best matching scan due to noise and other errors.

Two alternative approaches are employed in performing the four comparisons. These are discussed below in the following two subsections.

4.1.1 Least-Squares Approach

First, we estimate the angular position of the target as follows: Assuming the observed scan pattern is not saturated, we check if it has two humps or not. If so, it is a corner and we find the angular location of the dip in the middle of the two humps and the corresponding intensity value. If not, we find the angular location of the maximum, denoted θ_{MAX}, and again the corresponding intensity value. These angular values can be directly taken as estimates of the angular position of the target. Alternatively, the angular position can be estimated by

finding the center-of-gravity (COG) of the scan as follows:

$$\theta_{\mathrm{COG}} = \frac{\sum_{k=1}^{n} \alpha_k I(\alpha_k)}{\sum_{k=1}^{n} I(\alpha_k)} \tag{4.1}$$

where n is the number of samples in the angular scan. Ideally, these estimates would be equal, but in practice they differ by a small amount. We will consider the use of both alternatives when tabulating our results. From now on, we will refer to either estimate as the "center angle" of the scan.

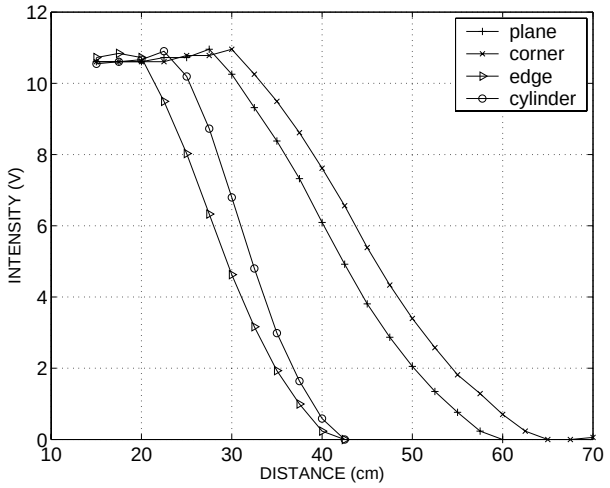

Figure 4.3: Central intensity versus distance curves for the different targets.

Plots of the intensity at the center angle of each scan in Figures 4.2(a)–(d) as a function of the distance at which that scan was obtained, play an important part in our method. Figure 4.3 shows these plots for the maximum intensity (central dip intensity for corner) case.

In this approach, we compare the intensity scan of the observed target with the four reference scans by computing their least-squares differences after aligning their centers with each other. Since the squared difference is sensitive even to multiplicative factors which are close to unity, we have employed a reference scan obtained by linearly interpolating between the two consecutive scans whose central intensities are just above and just below the observed scan. As shown in the figure, minimum value of the sum of the least-squares error corresponds to the correct target type. As expected from the intensity scans, the least-squares errors

for edge and cylinder are very similar and that for the corner differs significantly from the others due to its distinctive feature.

The least-squares difference between the observed scan and the four interpolated scans, one for each possible target type, is computed as follows:

$$\mathcal{E}_j = \sum_{i=1}^{n} [I(\alpha_i - \alpha_{\text{align}}) - I_j(\alpha_i)]^2 \tag{4.2}$$

where $I_j,\ j = 1, 2, 3, 4$ denote the four interpolated scans. Here, α_{align} is the angular shift which is necessary to align both scans. The target type resulting in the smallest value of $\mathcal{E}$ is declared as the observed target. An example plot of the least-squares errors between a planar target scan and the reference scans is given in Figure 4.4. Once the target type is determined, the range can be estimated by using linear interpolation on Figure 4.3. Note that, this way, the accuracy of the method is not limited by the 2.5 cm spacing used in collecting the reference scans.

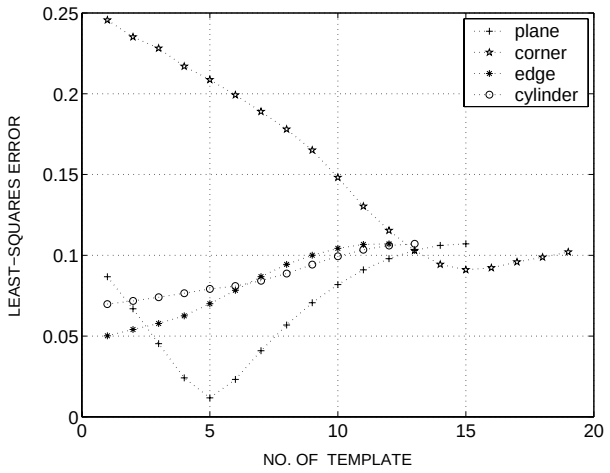

Figure 4.4: Least-squares errors between a planar target scan and the reference scans.

4.1.2 Matched Filtering Approach

As an alternative, we have also considered the use of matched filtering [49] to compare the observed and reference scans. A filter is matched to a signal $s(k)$ if

its impulse response $h(k)$ is given by

$$h(k) = s^*(-k) \tag{4.3}$$

where * denotes complex conjugation. When an input signal $g(k)$ is applied to this filter matched to a particular signal, then the output of the filter will be

$$v(k) = \sum_{l=-\infty}^{\infty} g(l)h(k-l) = \sum_{l=-\infty}^{\infty} g(l)s^*(l-k). \tag{4.4}$$

In our application, the output of the matched filter, the cross-correlation between the observed intensity scan and the jth reference scan, is normalized by the square root of its total energy:

$$y_j(l) = \frac{\sum_k I(\alpha_k) I_j(\alpha_{k-l})}{\sqrt{\sum_k [I_k(\alpha_k)]^2}} \tag{4.5}$$

The target type corresponding to the maximum cross-correlation is declared as the correct target type, and the angular position of the correlation peak directly provides an estimate of the azimuth angle of the target. Then, the distance is estimated by using linear interpolation on Figure 4.3 with the intensity value at the azimuth estimate.

4.1.3 Saturated Scans

If saturation is detected in the observed scan, special treatment is necessary. In the least-squares approach, the sum of squared differences between the aligned observed scan and *all* the saturated reference scans are computed and the target type with the minimum sum of squared differences is chosen. The range estimate of the target is taken as the distance corresponding to the scan resulting in the minimum sum of squared differences. Similarly, for the matched filter, correlation between the observed scan and *all* the stored saturated reference scans is computed and the target type resulting in the highest correlation peak is selected. Again, the angular position of the correlation peak is taken as the azimuth estimate of the target and the range estimate is again taken as that of the best matching scan.

It should be noted that, in the saturated case, range estimation accuracy is limited by the 2.5 cm interval at which the reference scans were taken since interpolation is not possible. If this accuracy is not satisfactory, it can be improved by reducing the 2.5 cm intervals. We underline that the 2.5 cm interval does not limit the range estimation accuracy in the unsaturated case, where accurate interpolation is possible from Figure 4.3.

4.1.4 Experimental Verification and Discussion

In this section, we experimentally verify the proposed method by locating the targets at randomly selected distances r and azimuth angles θ and collecting a total of 120 test scans. The targets are randomly located at azimuths varying from -45° to 45° from 15 cm up to the maximum ranges in Figures 4.2(a)–(d).

The results of least-squares based target differentiation are displayed in Tables 4.1 and 4.2 in the form of target confusion matrices. Table 4.1 gives the results obtained using the maximum (or the central dip for corner) intensity values, and Table 4.2 gives those obtained using the intensity value at the COG of the scans. The average accuracy over all target types can be found by summing the correct decisions given along the diagonal of the confusion matrix and dividing this sum by the total number of test trials (120). The average correct classification rates obtained by using the max/dip and the COG variations of the least-squares approach are 93% and 89%, respectively.

Matched filter differentiation results are presented in Table 4.3. The average accuracy of differentiation over all target types is 97% which is better than that obtained with the least-squares approach. The matched filter correctly classifies planar targets as well as corners with an accuracy of 100%.

As shown in the tables, corners are always correctly identified regardless of which method is used, due to their distinctive signature. Second best to corners are planes which are also usually correctly identified. Cylinders and edges are the most confused target types as we had expected from the similar nature of their

Table 4.1: Target confusion matrix: least-squares based classification (max/dip variation) (P: plane, C: corner, E: edge, CY: cylinder).

target	differentiation result				total
	P	C	E	CY	
P	29	–	1	–	30
C	–	30	–	–	30
E	1	–	26	3	30
CY	4	–	–	26	30
total	34	30	27	29	120

Table 4.2: Target confusion matrix: least-squares based classification (COG variation).

target	differentiation result				total
	P	C	E	CY	
P	30	–	–	–	30
C	–	30	–	–	30
E	5	–	23	2	30
CY	4	–	2	24	30
total	39	30	25	26	120

intensity scans. Nearly all misclassified targets are located at far ranges where the return signal intensities are very weak.

The average absolute range and azimuth estimation errors for the different approaches are presented in Table 4.4 over all test targets. As seen in the table, using the max/dip and COG variations of the least-squares approach, the target ranges are estimated with average absolute range errors of 1.2 cm and 1.7 cm, respectively. Matched filtering results in an average absolute range error of 0.8 cm which is much better than that obtained with the least-squares approach. The

Table 4.3: Target confusion matrix: matched filter based classification.

target	differentiation result				total
	P	C	E	CY	
P	30	–	–	–	30
C	–	30	–	–	30
E	–	–	29	1	30
CY	–	–	3	27	30
total	30	30	32	28	120

Table 4.4: Absolute range and azimuth estimation errors over all test targets.

method		P	C	E	CY	average error
least squares	r(cm)	1.0	0.7	1.1	1.8	1.2
(max/dip)	θ(deg)	4.1	5.7	2.3	1.7	3.5
least squares	r(cm)	0.5	0.7	4.3	1.5	1.7
(COG)	θ(deg)	2.9	2.8	3.0	2.4	2.8
matched	r(cm)	0.7	0.7	0.8	1.0	0.8
filter	θ(deg)	1.2	1.7	1.8	1.8	1.6

greatest contribution to the range errors comes from targets which are incorrectly differentiated. If we average over only correctly differentiated targets, the average absolute range errors are reduced to 0.6 cm, 0.6 cm, and 0.7 cm for the max/dip and COG variations of least-squares and the matched filter approaches, respectively. Since these numbers are comparable, we may conclude that the superior range accuracy of matched filtering is mostly a consequence of its superior differentiation accuracy.

As for azimuth estimation, matched filtering results in an average absolute estimation error of 1.6°, which is the best among the approaches compared. Averaging the azimuth errors over only correctly differentiated targets does not

result in significant changes. This is due to the fact that azimuth estimation is not dependent on correct differentiation.

Because of the sharpness of the scans for the cylindrical target around their peaks, azimuth estimation of cylinders is more accurate than that of other targets when the least-squares approach is used. On the other hand, angular localization of corners is less accurate since it is difficult to estimate with good accuracy the exact angular location of the relatively shallow central dip, especially with the max/dip variation of the least-squares approach. The COG variation is, on the average, better than the max/dip variation in azimuth estimation due to the fact that COG based calculations average out the noise in the return signal intensities.

4.2 Position-Invariant Surface Recognition and Localization

In this section, we consider the use of the same infrared system as in Section 4.1, for the purpose of surface recognition and localization [50]. In this case, the target geometry is kept fixed but its surface properties vary. This section complements the work presented in Section 4.1 where we considered the differentiation and localization of targets with different geometries such as plane, corner, edge, and cylinder [51].

The surfaces employed in this study are aluminum, white painted wall, brown craft paper, styrofoam packaging material, blister packaging material, and unfinished wood. Our method, similar described to that in Section 4.1, is based on angularly scanning the surfaces over a certain angular range. Reference data sets are collected for each surface type at $\theta = 0^\circ$ with 2.5 cm distance increments, ranging from 12.5 cm to 57.5 cm.

The resulting reference scans for the six surfaces are shown in Figure 4.5. As we will see, these scans contain sufficient information to identify and localize different surfaces with a good degree of accuracy. Notice that the return signal

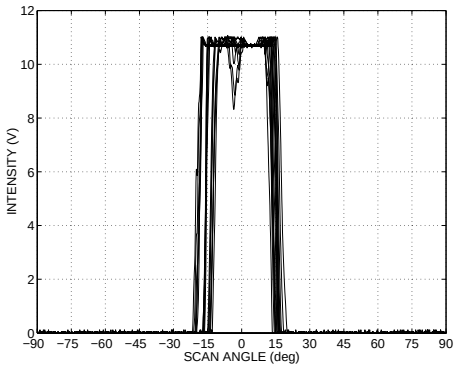

(a) aluminum

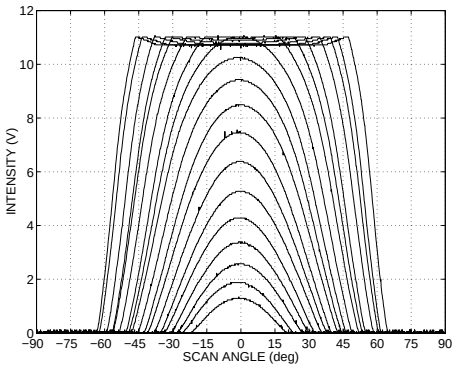

(b) white painted wall

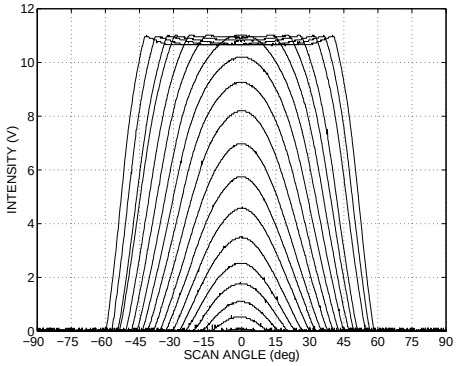

(c) brown craft paper

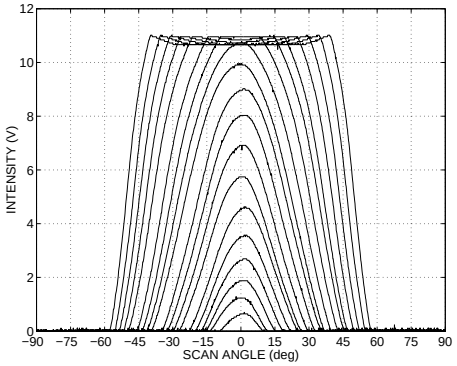

(d) styrofoam packaging material

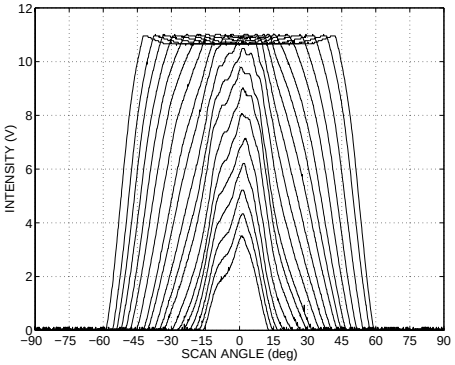

(e) blister packaging material

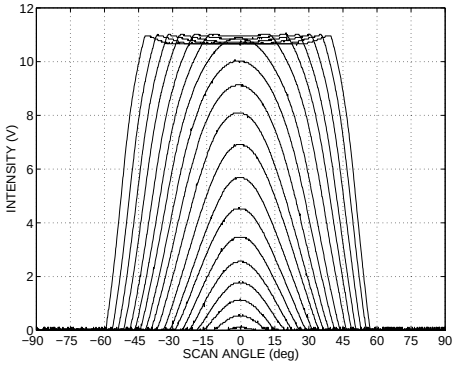

(f) wood

Figure 4.5: Intensity scans of the various surfaces at various distances.

intensities saturate at an intensity corresponding to 10.7 V output voltage as before.

4.2.1 The Method

We now describe briefly how to recognize and determine the position of an arbitrarily located surface whose intensity scan has been observed. First, we check whether the observed scan $I(\alpha)$ exhibits saturation or not. Saturated scans are treated in the same manner as in Section 4.1.3. Due to the similar properties of the observed intensity scans to the scans obtained from targets of different geometries, we applied the same procedure in Section 4.1. We compare the unsaturated observed scan not with all scans at all distances but only with the four (one for each surface type) reference scans obtained by linearly interpolating between the two consecutive scans whose central intensities are just above and just below the observed scan.

As alternatives, we tested our method by comparing the observed scan with *eight* scans whose nearest central intensities are both above *and* below the observed central intensity, and with *all* scans included in each of the two groups of surfaces considered in Section 4.2.1. These computationally more expensive approaches, exceedingly more so in the latter case, did not result in any improvement, when compared with only four scans. Furthermore, the results obtained by using all scans are found to be inferior to those obtained by using four scans due to noise and other errors, which result in misclassification.

Plots of the intensity at the center angle of each scan in Figure 4.5 as a function of the distance at which that scan was obtained, are used in range estimation for unsaturated scans. Figure 4.6 shows these plots for the maximum intensity case.

Again, two alternative approaches, least-squares and matched filtering, whose details are discussed in Sections 4.1.1 and 4.1.2 are employed in performing the four comparisons.

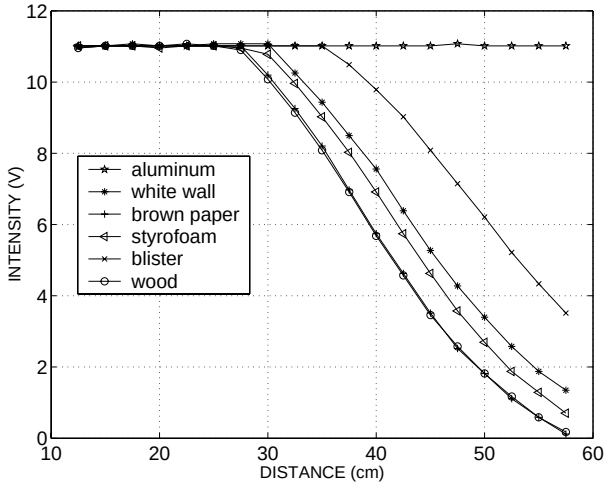

Figure 4.6: Central intensity versus distance curves for the different surfaces.

4.2.2 Experimental Verification and Discussion

In this section, we experimentally verify the proposed method by locating the surfaces at randomly selected distances r and azimuth angles θ and collecting a total of 100 test scans. The surfaces are randomly located at ranges from 12.5 cm up to 57.5 cm and azimuths from $-45°$ to $45°$. Two groups of surfaces are considered: aluminum, white painted wall, brown craft paper, and styrofoam packaging material are included in the first group, and aluminum, white painted wall, blister packaging material, and wood are included in the second group. As the number of surfaces increases, the correct differentiation rates decrease as expected from the nature of the intensity scans. Taking this into consideration, we chose these two groups of surfaces.

The results of least-squares based surface differentiation are displayed in Tables 4.5 and 4.6 in the form of confusion matrices for the surfaces included in the first group. Table 4.5 gives the results obtained using the maximum intensity values, and Table 4.6 gives those obtained using the intensity value at the COG of the scans. The average accuracy over all target types can be found by summing the correct decisions given along the diagonal of the confusion matrix and dividing this sum by the total number of test trials (100). The average correct classification rates obtained by using the maximum intensity and the COG

variations of the least-squares approach are 83% and 82%, respectively.

Table 4.5: Surface confusion matrix: least-squares based recognition (maximum intensity variation) (AL: aluminum, WW: white wall, BP: brown paper, ST: styrofoam).

surface	recognition result				total
	AL	WW	BP	ST	
AL	25	–	–	–	25
WW	–	20	3	2	25
BP	–	2	19	4	25
ST	–	–	6	19	25
total	25	22	28	25	100

Table 4.6: Surface confusion matrix: least-squares based recognition (COG variation).

surface	recognition result				total
	AL	WW	BP	ST	
AL	25	–	–	–	25
WW	–	20	3	2	25
BP	–	4	18	3	25
ST	–	–	6	19	25
total	25	24	27	24	100

Matched filter differentiation results are presented in Table 4.7. The average accuracy of differentiation over all surfaces is 87%, which is better than that obtained with the least-squares approach. In [51], where we dealt with the differentiation of targets with different geometries as opposed to different surface properties treated here, the least-squares approach resulted in a differentiation accuracy of 93% and 89% and the matched filtering approach resulted in an accuracy of 97%. Based on these results, we conclude that differentiating targets

with different surfaces is considerably more difficult than differentiating targets with different geometries.

Table 4.7: Surface confusion matrix: matched filter based recognition.

surface	recognition result				total
	AL	WW	BP	ST	
AL	25	–	–	–	25
WW	–	21	3	1	25
BP	–	1	21	3	25
ST	–	–	5	20	25
total	25	22	29	24	100

As shown in the tables, aluminum is always correctly identified regardless of which method is used, due to its distinctive signature. The remaining surfaces are comparable in terms of their correct identification percentages. Brown craft paper and styrofoam are the surfaces most confused with each other. Although the intensity scans of these two surfaces do not resemble each other in the unsaturated region, their saturated scans are similar, contributing to the misclassification rate. Nearly all misclassified surfaces are located at nearby ranges where the return signal intensities are saturated. This means that the misclassification rate can be reduced by increasing the lower limit of the range interval at the cost of reducing the operating range.

The average absolute range and azimuth estimation errors for the different approaches are presented in Table 4.8 over the surface types in the first group. As seen in the table, using the maximum intensity and COG variations of the least-squares approach, the target ranges are estimated with average absolute range errors of 1.4 cm and 1.5 cm, respectively. Matched filtering results in an average absolute range error of 1.2 cm which is better than that obtained with the least-squares approach. The greatest contribution to the range errors comes from targets which are incorrectly recognized. If we average over only correctly recognized targets, the average absolute range errors become 1.0 cm, 1.1 cm, and

1.2 cm for the maximum intensity and COG variations of least-squares and the matched filter approaches, respectively. Since these three numbers are relatively closer than the corresponding numbers in Table 4.8, we may conclude that the superior range accuracy of matched filtering is mostly a consequence of its superior differentiation accuracy.

Table 4.8: Absolute range and azimuth estimation errors over the surfaces included in the first group.

method		AL	WW	BP	ST	average error
least squares	r(cm)	2.4	1.3	0.9	0.9	1.4
(max)	θ(deg)	0.8	1.9	1.6	0.8	1.3
least squares	r(cm)	2.4	1.3	1.3	0.9	1.5
(COG)	θ(deg)	0.8	1.0	1.6	0.8	1.1
matched	r(cm)	1.7	1.2	1.0	0.8	1.2
filter	θ(deg)	0.8	1.1	1.6	0.7	1.0

The major contribution to range errors comes from saturated scans where linear interpolation from Figure 4.6 cannot be employed to obtain better range estimates. Consequently, surfaces for which saturation occurs over a greater portion of the operating range exhibit greater range estimation errors, with aluminum being the worst.

As for azimuth estimation, matched filtering results in an average absolute estimation error of 1.0°, which is the best among the approaches compared. Averaging the azimuth errors over only correctly differentiated surfaces does not result in significant changes. This is due to the fact that azimuth estimation is not dependent on correct differentiation. The COG variation is, on the average, better than the maximum intensity variation in azimuth estimation due to the fact that COG based calculations average out the noise in the return signal intensities.

We have also considered expanding the range of operation of the system. As

an example, changing the operating range from [12.5 cm, 57.5 cm] to [5 cm, 60 cm] results in a reduction of the correct differentiation percentage from 87% to 80%. This reduction in performance is mostly a consequence of highly saturated scans and scans with very low intensities, both of which are prone to greater errors.

The results of least-squares based surface differentiation are displayed in Tables 4.9 and 4.10 in the form of confusion matrices for the surfaces included in the second group. Table 4.9 gives the results obtained using the maximum intensity values, and Table 4.10 gives those obtained using the intensity value at the COG of the scans. The average correct classification rates obtained by using the maximum intensity and the COG variations of the least-squares approach are 83% and 82%, respectively.

Table 4.9: Surface confusion matrix: least-squares based classification (maximum intensity variation) (AL: aluminum, WW: white painted wall, WD: wood, BM: blister packaging material).

surface	differentiation result				total
	AL	WW	WD	BM	
AL	25	–	–	–	25
WW	–	19	6	–	25
WD	–	–	20	5	25
BM	–	–	6	19	25
total	25	19	32	24	100

Matched filter differentiation results are presented in Table 4.11. The average accuracy of differentiation over all surfaces is 86%, which is better than that obtained with the least-squares approach.

As shown in the tables, aluminum is always correctly identified regardless of which method is used, due to its distinctive signature. White painted wall is better classified with matched filtering approach than with least-squares approach. Wood and blister packaging material are the most confused surfaces. Although their intensity patterns do not resemble each other in the unsaturated region,

Table 4.10: Surface confusion matrix: least-squares based classification (COG variation).

surface	differentiation result				total
	AL	WW	WD	BM	
AL	25	–	–	–	25
WW	–	19	6	–	25
WD	–	1	19	5	25
BM	–		6	19	25
total	25	20	31	24	100

Table 4.11: Surface confusion matrix: matched filter based classification.

surface	differentiation result				total
	AL	WW	WD	BM	
AL	25	–	–	–	25
WW	–	23	2	–	25
WD	–	–	19	6	25
BM	–	–	6	19	25
total	25	23	27	25	100

their saturated patterns are similar, resulting in misclassification. Nearly all misclassified targets are located at nearby ranges where the return signal intensities are saturated.

The average absolute range and azimuth estimation errors for the different approaches are presented in Table 4.12 over the surface types included in the second group. As seen in the table, using the maximum intensity and COG variations of the least-squares approach, the target ranges are estimated with an average absolute range error of 1.4 cm in both cases. Matched filtering results in an average absolute range error of 1.0 cm which is better than that obtained with the least-squares approach. The greatest contribution to the range error comes

Table 4.12: Absolute range and azimuth estimation errors over the surfaces included in the second group.

method		AL	WW	WD	BM	average error
least squares	r(cm)	2.4	1.6	0.6	0.9	1.4
(max)	θ(deg)	0.8	1.9	2.6	1.2	1.6
least squares	r(cm)	2.4	1.6	0.8	0.8	1.4
(COG)	θ(deg)	0.8	1.0	1.5	0.8	1.0
matched	r(cm)	1.7	0.9	0.5	0.8	1.0
filter	θ(deg)	0.8	1.0	1.0	0.7	0.9

from targets which are incorrectly recognized. If we average over only correctly differentiated targets, the average absolute range errors are reduced to 0.9 cm, 1.1 cm, and 0.8 cm for the maximum intensity and COG variations of least-squares and the matched filter approaches, respectively. Since these numbers are comparable, we may conclude that the superior range accuracy of matched filtering is mostly a consequence of its superior differentiation accuracy as before.

The major contribution to range errors comes from saturated scans where linear interpolation does not provide better range estimates from Figure 4.6. In the least-squares approach, aluminum is located with an absolute range error of 2.4 cm. As seen in Figure 4.5(a), the reference scans for aluminum do not show great differences with the change in the range, which prevents a better range estimation.

As for azimuth estimation, matched filtering results in an average absolute estimation error of 0.9°, which is the best among the approaches compared. Averaging the azimuth errors over only correctly differentiated surfaces does not result in significant changes. The COG variation is, on the average, better than the maximum intensity variation in azimuth estimation due to the fact that COG based calculations average out the noise in the return signal intensities.

We have also considered expanding the range of operation of the system. As

an example, changing the operating range from [12.5 cm, 57.5 cm] to [5 cm, 60 cm] results in a reduction of the correct differentiation percentage from 86% to 79%. This reduction in performance is mostly a consequence of highly saturated scans and scans with very low intensities, both of which which are prone to greater errors in differentiation.

Light reflected from a surface consists of both specular and diffuse components. The specular component is concentrated where the reflection angle equals the incidence angle, whereas the diffuse component is spread in all directions with a cosine factor. For different types of surfaces, the contribution of these two components and the rate of decrease of intensity with the scan angle α is different. It is this difference which results in a characteristic intensity scan pattern (signature) for each target, enabling us to distinguish them without knowing their positions. In contrast, a system relying only on reflected energy could not distinguish between a highly reflecting distant object and a less reflecting nearby one. Occasionally, two very distinct surfaces may have intensity scans with very similar dependence on α, in which case they cannot be reliably differentiated with the present method.

In this chapter, we considered the differentiation and localization of targets having different geometries such as plane, corner, edge, and cylinder but fixed surface properties (Section 4.1) and targets having different surface properties but fixed geometric shape (Section 4.2). 97% correct differentiation was achieved in the first case and correct differentiation rates of 87% and 86% over the two groups of surfaces are achieved in the latter case. Comparing these correct differentiation rates, we conclude that surface characteristics are not as distinctive as geometric reflection characteristics of targets.

The method we propose is scalable in the sense that the accuracy can be increased by increasing the number of reference scans without increasing the computational cost.

Chapter 5

DIFFERENTIATION AND LOCALIZATION OF GENERALIZED TARGETS

In Chapter 4, we considered targets having either different geometries but fixed surface properties, or targets with different surface properties but fixed geometries. In this chapter, we treat the combination of a particular geometry and particular surface as a generalized target type and apply the methods explained in detail in Chapter 4. Plane, 90° corner, and 90° edge covered with aluminum, styrofoam packaging material, white cloth, and white drawing paper are employed as generalized targets. The resulting reference scans for these targets obtained with the experimental setup (Figure 4.1) are presented in Figures 5.1– 5.3. The intensity scans of the corner covered with aluminum have three humps which differ significantly from those of corners of other surface types where a double-humped scan pattern is observed. This distinctive feature is used in the differentiation of corners covered with aluminum. Scans of corner targets with surfaces other than aluminum also have a triple-humped pattern (with a much smaller middle hump) corresponding to two orthogonal constituent planes and their intersections which was not observed explicitly in the scan patterns of wooden corners. Greatest difficulty is encountered in differentiating edges of different surfaces which have

the most similar intensity patterns.

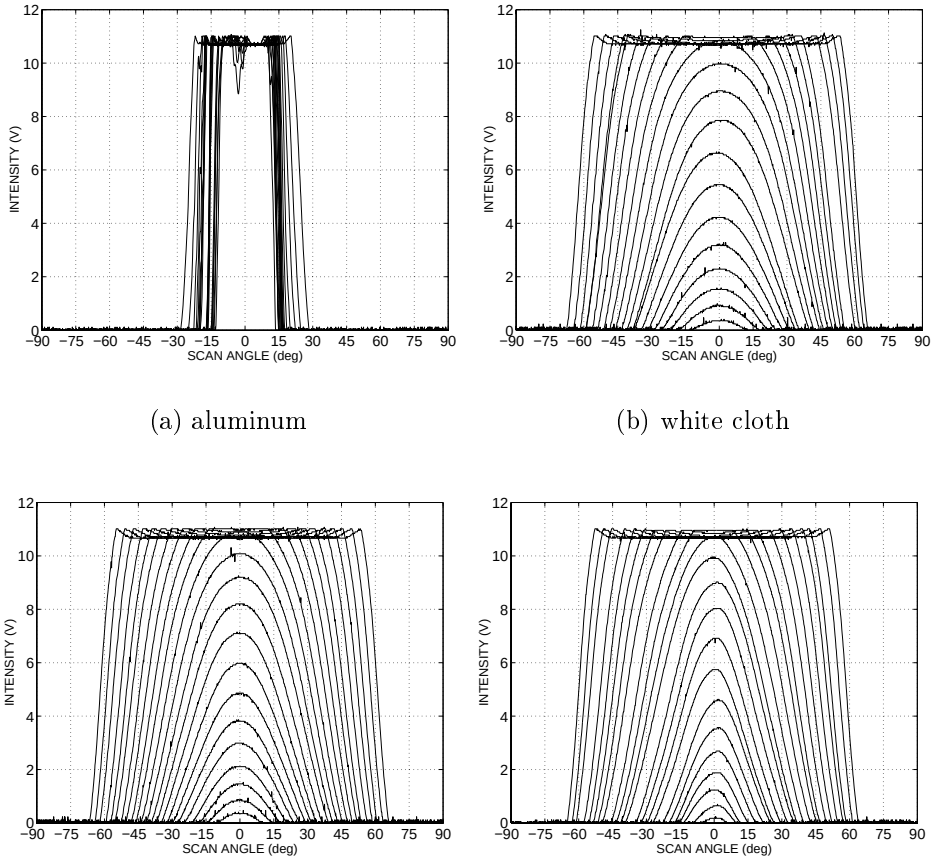

(a) aluminum

(b) white cloth

(c) white drawing paper

(d) styrofoam packaging material

Figure 5.1: Intensity scans of planes of different surface types at various distances.

5.1 The Method

We now describe the differentiation process briefly. First, we check whether the observed intensity scan has three distinct humps or not. If so, the target is a corner covered with aluminum, and the same procedure for saturated scans explained in Section 4.1.3 is applied for the differentiation and localization of these targets. For the other targets, similar differentiation and localization approaches

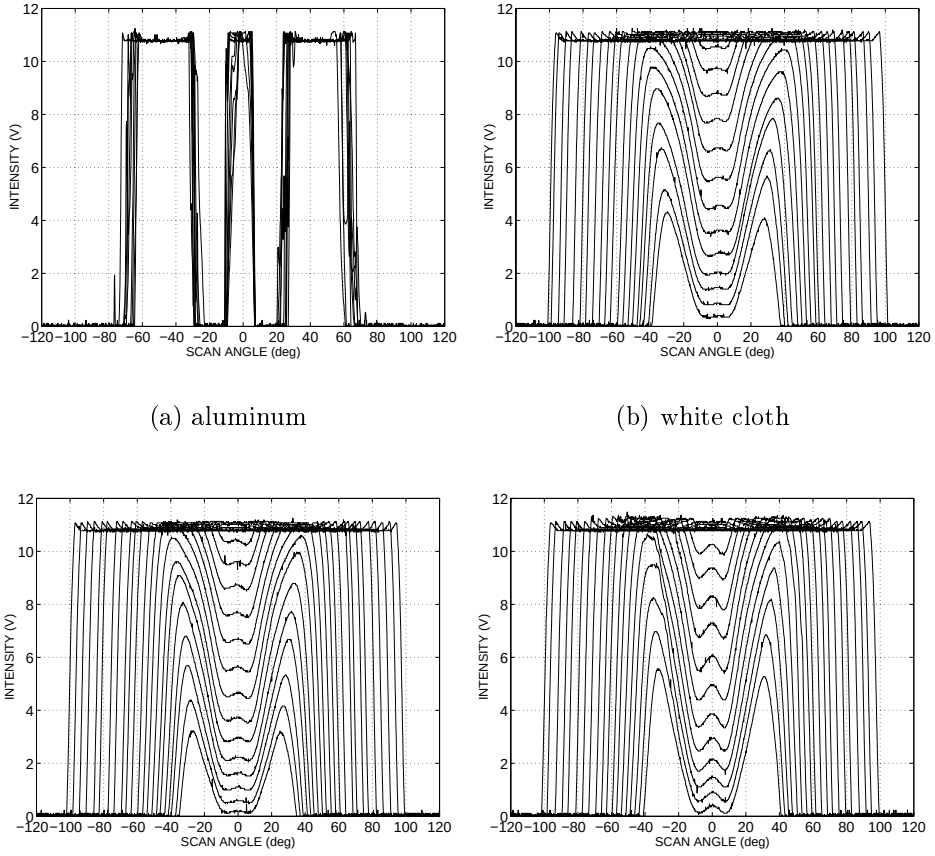

(a) aluminum

(b) white cloth

(c) white drawing paper

(d) styrofoam packaging material

Figure 5.2: Intensity scans of corners of different surface types at various distances.

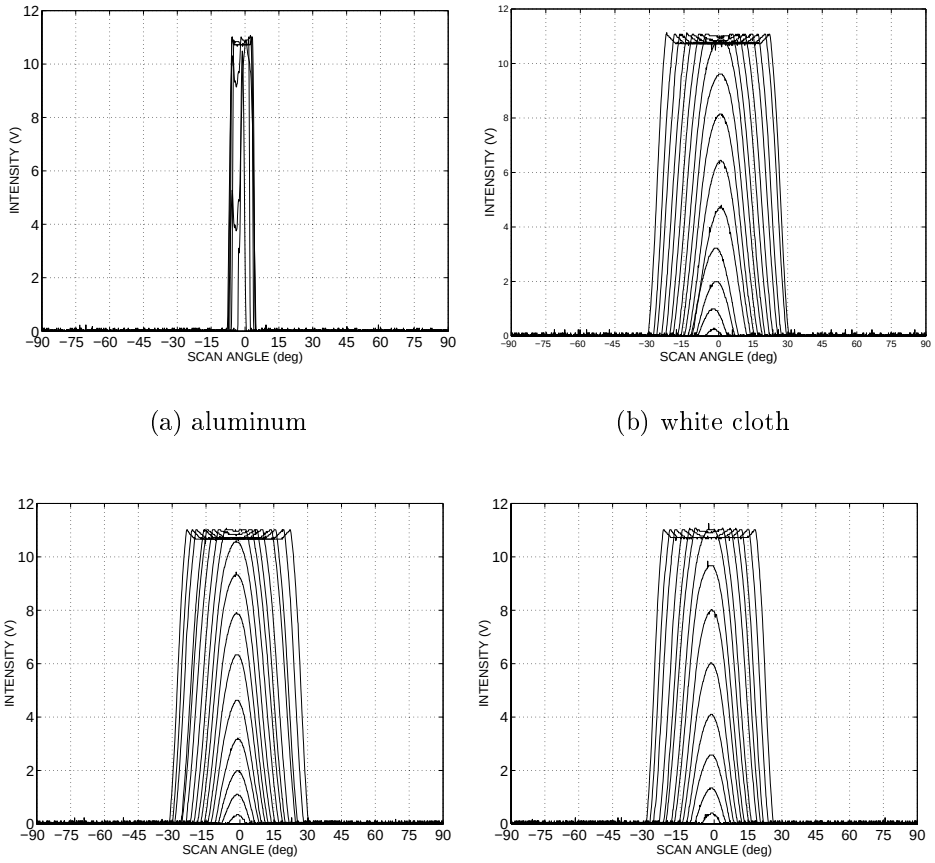

(a) aluminum

(b) white cloth

(c) white drawing paper

(d) styrofoam packaging material

Figure 5.3: Intensity scans of edges of different surface properties at various distances.

as in Chapter 4 are applied. In the max/center variation of least-squares approach, we find the angular location of the corner by taking the average of the angular locations of the two humps of the intensity scans. For unsaturated scans, we compare the observed scan with the twelve scans (one for each particular geometry and surface type). Once the target type is determined, the range can be estimated by using linear interpolation on Figure 5.4.

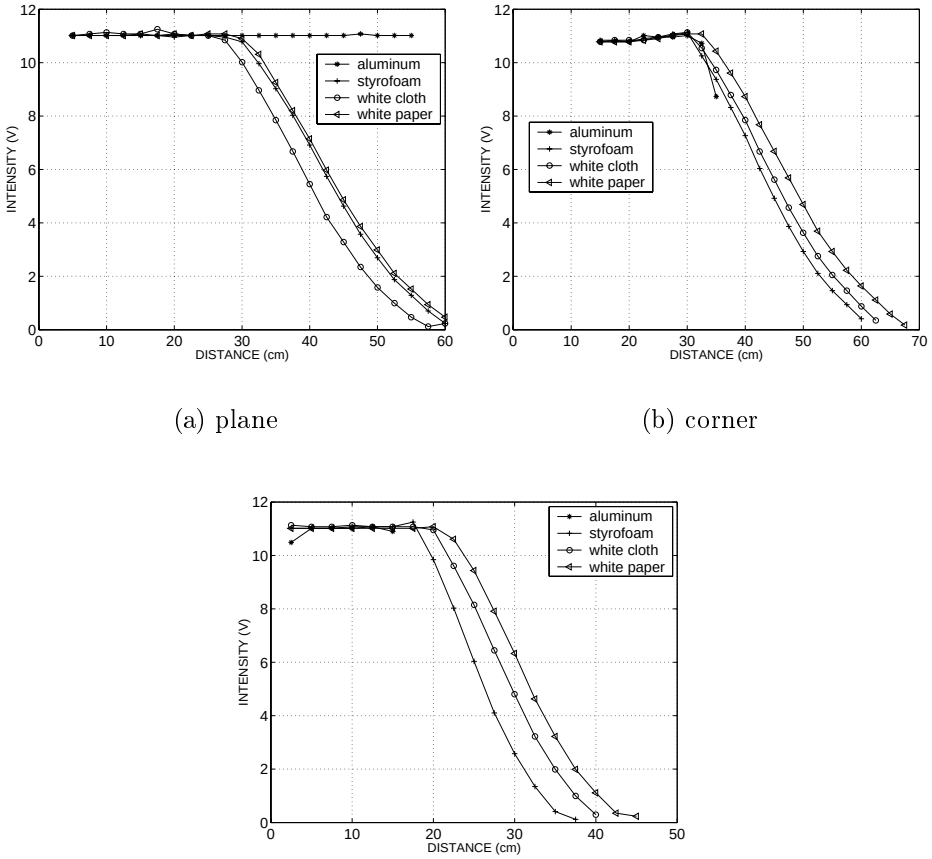

(a) plane

(b) corner

(c) edge

Figure 5.4: Intensity versus distance for targets of different geometries.

5.2 Experimental Verification and Discussion

In this section, we experimentally verify the proposed method. First, reference data sets are collected for each target with 2.5 cm distance increments, from their nearest observable range to their maximum observable range, at $\theta = 0°$. Then, a total of 273 test scans are collected by locating the targets at randomly selected distances and azimuth angles (r, θ).

Table 5.1: Confusion matrix: least-squares based classification (max/center variation) (AL: aluminum, WC: white cloth, WP: white paper, ST: styrofoam).

surface	differentiation result												total
	plane				corner				edge				
	AL	WC	WP	ST	AL	WC	WP	ST	AL	WC	WP	ST	
AL	24	–	–	–	–	–	–	–	–	–	–	–	24
WC	–	18	9	3	–	–	–	–	–	–	–	–	30
WP	–	3	21	6	–	–	–	–	–	–	–	–	30
ST	–	2	8	20	–	–	–	–	–	–	–	–	30
AL	–	–	–	–	22	–	–	–	–	–	–	–	22
WC	–	–	–	–	–	9	3	10	–	–	–	–	22
WP	–	–	–	–	–	1	15	5	–	–	–	–	21
ST	–	–	–	–	1	–	2	18	–	–	–	–	21
AL	–	–	–	1	–	–	–	–	7	–	1	1	10
WC	–	–	–	–	–	–	–	–	–	9	6	5	20
WP	–	–	–	1	–	–	–	–	–	10	5	7	23
ST	–	2	–	–	–	–	–	–	–	7	8	3	20
total	24	25	38	31	23	10	20	33	7	26	20	16	273

The results of least-squares based target differentiation are displayed in Tables 5.1 and 5.2 in the form of confusion matrices. Table 5.1 gives the results obtained using the maximum/center intensity values, and Table 5.2 gives those obtained using the intensity value at the COG of the scans. The average accuracy over all target types can be found by summing the correct decisions given along the diagonal of the confusion matrix and dividing this sum by the total number of test trials (273).

The average correct classification rates obtained by using the max/center and

Table 5.2: Confusion matrix: least-squares based classification (COG variation).

surface	differentiation result												total
	plane				corner				edge				
	AL	WC	WP	ST	AL	WC	WP	ST	AL	WC	WP	ST	
AL	24	–	–	–	–	–	–	–	–	–	–	–	24
WC	–	19	9	2	–	–	–	–	–	–	–	–	30
WP	–	4	21	5	–	–	–	–	–	–	–	–	30
ST	–	2	8	20	–	–	–	–	–	–	–	–	30
AL	–	–	–	–	22	–	–	–	–	–	–	–	22
WC	–	–	–	–	–	11	4	7	–	–	–	–	22
WP	–	–	–	–	–	5	11	5	–	–	–	–	21
ST	–	–	–	–	1	2	2	16	–	–	–	–	21
AL	–	–	1	–	–	–	–	–	7	–	1	1	10
WC	–	–	–	–	–	–	–	–	–	13	1	6	20
WP	–	1	1	–	–	–	–	–	–	13	–	8	23
ST	–	2	2	–	–	–	–	–	–	10	1	5	20
total	24	28	42	27	23	18	17	28	7	36	3	20	273

Table 5.3: Confusion matrix: matched filter based classification.

surface	differentiation result												total
	plane				corner				edge				
	AL	WC	WP	ST	AL	WC	WP	ST	AL	WC	WP	ST	
AL	24	–	–	–	–	–	–	–	–	–	–	–	24
WC	–	22	6	1	–	–	–	–	–	–	1	–	30
WP	–	–	23	7	–	–	–	–	–	–	–	–	30
ST	–	–	8	21	–	–	–	–	–	1	–	–	30
AL	–	–	–	–	22	–	–	–	–	–	–	–	22
WC	–	–	–	–	–	13	5	4	–	–	–	–	22
WP	–	–	–	–	–	4	15	2	–	–	–	–	21
ST	–	–	–	–	1	4	3	13	–	–	–	–	21
AL	–	–	–	–	–	–	–	–	9	1	–	–	10
WC	–	–	–	–	–	–	–	–		6	7	7	20
WP	–	–	–	2	–	–	–	–		9	3	9	23
ST	–	–	–	2	–	–	–	–	1	5	6	6	20
total	24	22	37	33	23	21	23	19	10	22	17	22	273

Table 5.4: Absolute range and azimuth estimation errors over all test targets (LS: least squares, MF: matched filter).

		plane				corner				edge				
method		AL	WC	WP	ST	AL	WC	WP	ST	AL	WC	WP	ST	av. error
LS	r(cm)	2.2	2.5	2.6	2.5	2.1	0.9	0.6	1.0	7.6	1.8	2.8	5.4	2.7
(max/center)	θ(deg)	0.9	3.1	1.3	4.4	2.3	1.8	1.4	1.4	1.8	2.0	1.8	7.3	2.5
LS	r(cm)	2.2	0.8	0.9	0.9	2.1	0.8	1.1	1.1	4.3	1.4	3.6	4.7	2.0
(COG)	θ(deg)	0.9	1.4	0.9	0.9	2.3	1.4	1.2	1.1	1.2	2.2	2.9	4.2	1.7
MF	r(cm)	1.7	0.9	2.6	2.5	1.5	0.7	0.8	2.3	2.2	2.0	4.1	6.4	2.3
	θ(deg)	0.8	1.2	0.7	0.7	1.0	1.0	0.7	2.4	1.1	2.8	1.3	2.6	1.4

the COG variations of the least-squares approach are 63% and 62%, respectively.

Matched filter differentiation results are presented in Table 5.3. The average accuracy of differentiation over all target types is 65% which is better than that obtained with the least-squares approach.

Planes and corners covered with aluminum are correctly classified with all approaches employed due to their distinctive features. Planar targets of different surface properties are better classified than the others, with correct differentiation rates of 73%, 74% and 79% for the max/center and the COG variations of the least-squares and matched filter approaches, respectively. As expected from the intensity scans, it is difficult to differentiate edges of different surface properties. The highest correct differentiation rate of 34% for edges is achieved in the COG variation of the least-squares approach.

The average absolute range and azimuth estimation errors for the different approaches are presented in Table 5.4 over all test targets. As seen in the table, using the max/center and COG variations of the least-squares approach, the target ranges are estimated with average absolute range errors of 2.7 cm and 2.0 cm, respectively. Matched filtering results in an average absolute range error of 2.3 cm which is comparable with least squares. The greatest contribution to the range errors comes from targets which are incorrectly differentiated and whose intensity scans are saturated.

As for azimuth estimation, matched filtering results in an average absolute estimation error of 1.4°, which is the best among the approaches compared.

In this chapter, we considered the differentiation and localization of targets having both different geometrical shapes and surface properties. 65% correct differentiation rate was achieved. When we compare this rate with the correct differentiation rates achieved in Chapter 4, we can conclude that it is much more difficult to differentiate targets of different surface properties than targets of different geometrical shapes.

Chapter 6

CONCLUSIONS and FUTURE WORK

In this thesis, different approaches are presented for the differentiation and localization of targets using low-cost infrared sensors. These rule-based and template-based differentiation and localization approaches can handle a moderate number of targets of different geometries and surface properties.

The effect of parameters such as range, azimuth, and surface properties of the targets on the correct differentiation and localization performance have been investigated and the different approaches are compared.

The accuracy of the template-based algorithms depends on the similarity of the observed intensity scans of the targets. As shown in the thesis, surface properties of the targets are not as distinctive as their geometrical shapes. Therefore, provided that the surface properties of the targets are not very similar, our approaches can reliably differentiate and localize targets in a position-invariant manner. The methods are scalable in the sense that the accuracy can be increased by increasing the number of reference scans without increasing the computational cost.

Future work may involve developing parametric models based on physical

reflection models for the intensity scans which would enable more direct determination of the target type and position. Ways to improve the accuracy of the methods, especially for targets of different geometries and surface properties will be sought. Instead of symmetrical targets as used in our study, imperfect targets or objects with arbitrary shapes will be considered. The performance of the methods discussed in this thesis will also be tested and evaluated in our laboratory on a small mobile robot for map building in a test room composed of primitive target types considered in this study.

The main contribution of this thesis is that even though the intensity patterns are highly dependent on the geometrical shape, location and surface properties of the target, and this dependence cannot be represented by a simple relationship, we achieved position-invariant target differentiation. We have also shown that geometric properties of the targets are more distinctive than their surface properties.

The results indicate that simple infrared sensors, when coupled with appropriate processing, can be used to extract a significantly greater amount of information than they are commonly employed for.

Bibliography

[1] P. J. Phillips, "Matching pursuit filters applied to face identification," *IEEE Transactions on Image Processing*, vol. 7, no. 8, pp. 1150–1164, August 1998.

[2] L. Kwon, S. Z. Der, and N. M. Nasrabadi, "Adaptive multisensor target detection using feature-based fusion," *Optical Engineering*, vol. 41, no. 1, pp. 69–80, January 2002.

[3] T. Tsao and Z. Q. Wen, "Image-based target tracking through rapid sensor orientation change," *Optical Engineering*, vol. 41, no. 3, pp. 697–703, March 2002.

[4] I. Pavlidis, P. Symosek, B. Fritz, M. Bazakos, and N. Papanikolopoulos, "Automatic detection of vehicle occupants: the imaging problem and its solution," *Machine Vision and Applications*, vol. 11, no. 6, pp. 313–320, April 2000.

[5] P. M. Tag, R. L. Bankert, and L. R. Brody, "An AVHRR multiple cloud-type classification package," *Journal of Applied Meteorology*, vol. 39, no. 2, pp. 125–134, February 2000.

[6] A. K. Jain, N. K. Ratha, and S. Lakshmanan, "Object detection using Gabor filters," *Pattern Recognition*, vol. 30, no. 2, pp. 295–309, February 1997.

[7] Z. Zalevsky, D. Mendlovic, E. Rivlin, and S. Rotman, "Contrasted statistical processing algorithm for obtaining improved target detection performances in infrared cluttered environment," *Optical Engineering*, vol. 39, no. 10, pp. 2609–2617, October 2000.

[8] B. Bhanu, P. Symosek, and S. Das, "Analysis of terrain using multispectral images," *Pattern Recognition*, vol. 30, no. 2, pp. 197–215, February 1997.

[9] F. T. S. Yu and S. Jutamulia, ed., *Optical Pattern Recognition*, Cambridge: Cambridge University Press, 1998.

[10] F. T. S. Yu and S. Yin, ed., *Selected Papers on Optical Pattern Recognition*, vol. MS 156 of *SPIE Milestone Series*, Bellingham, Washington: SPIE Optical Engineering Press, 1999.

[11] D. Casasent and D. Psaltis, "Scale invariant optical correlation using Mellin transforms," *Optics Communications*, vol. 17, no. 1, pp. 59–63, April 1976.

[12] M. McDonnell, "Clarification on use of Mellin transform in optical pattern recognition," *Optics Communications*, vol. 25, no. 3, pp. 320–322, 1978.

[13] H. H. Arsenault, Y. N. Hsu, and K. Chalasinska-Macukow, "Rotation-invariant pattern recognition," *Optical Engineering*, vol. 23, no. 6, pp. 705–709, November/December 1984.

[14] F. T. S. Yu, X. Li, E. Tam, S. Jutamulia, and D. A. Gregory, "Rotation invariant pattern recognition with a programmable joint transform correlator," *Applied Optics*, vol. 28, no. 22, pp. 4725–4727, 15 November 1989.

[15] G. Gheen, "Design considerations for low-clutter, distortion invariant correlation filters," *Optical Engineering*, vol. 29, no. 9, pp. 1029–1032, September 1990.

[16] C. Gu, J. Hong, and S. Campbell, "2-D shift invariant volume holographic correlator," *Optics Communications*, vol. 88, no. 4–6, pp. 309–314, 1 April 1992.

[17] A. Lohmann, Z. Zalevsky, and D. Mendlovic, "Synthesis of pattern recognition filters for fractional Fourier processing," *Optics Communications*, vol. 128, no. 4–6, pp. 199–204, 15 July 1996.

[18] P. Refregier, "Optical pattern recognition—optimal trade-off circular harmonic filters," *Optics Communications*, vol. 86, no. 2, pp. 113–118, 1 November 1991.

[19] K. Hashimoto, C. Kawaguchi, S. Matsueda, K. Morinaka, and N. Yoshiike, "People counting system using multisensing application," *Sensors and Actuators A—Physical*, vol. 66, pp. 50–55, 1998.

[20] A. J. Hand, "Infrared sensor counts insects," *Photonics Spectra*, vol. 32, no. 11, pp. 30–31, November 1998.

[21] H. C. Wikle, S. Kottilingam, R. H. Zee, and B. A. Chin, "Infrared sensing techniques for penetration depth control of the submerged arc welding process," *Journal of Materials Processing Technology*, vol. 113, no. 1–3, pp. 228–233, 15 June 2001.

[22] B. Butkiewicz, "Position control system with fuzzy microprocessor AL220," *Lecture Notes in Computer Science*, vol. 1226, pp. 74–81, 1997.

[23] H. R. Everett, *Sensors for Mobile Robots, Theory and Application*. 289 Linden St., Wellesley, MA: A K Peters, Ltd., 1995.

[24] G. Beccari, S. Caselli, and F. Zanichelli, "Qualitative spatial representations from task-oriented perception and exploratory behaviors," *Robotics and Autonomous Systems*, vol. 25, no. 3/4, pp. 147–157, 30 November 1998.

[25] A. Warszawski, Y. Rosenfeld, and I. Shohet, "Autonomous mapping system for an interior finishing robot," *Journal of Computing in Civil Engineering*, vol. 10, pp. 67–77, 1996.

[26] E. P. Lopes, E. P. L. Aude, J. T. C. Silveria, H. Serderia, and M. F. Martins, "Application of a blind person strategy for obstacle avoidance with the use of potential fields," *Proceedings of IEEE International Conference on Robotics and Automation*, vol. 3, pp. 2911–2916, 2001, Seoul, South Korea.

[27] A. M. Flynn, "Combining sonar and infrared sensors for mobile robot navigation," *International Journal of Robotics Research*, vol. 7, no. 6, pp. 5–14, December 1988.

[28] H. M. Barberá, A. G. Skarmeta, M. Z. Izquierdo, and J. B. Blaya, "Neural networks for sonar and infrared sensors fusion," *Proceedings of the Third*

International Conference on Information Fusion, vol. 2, pp. 18–25, 2000, France.

[29] A. M. Sabatini, V. Genovese, E. Guglielmelli, A. Mantuano, G. Ratti, and P. Dario, "A low-cost, composite sensor array combining ultrasonic and infrared proximity sensors," *Proceedings of the IEEE/RSJ International Conference on Intelligent Robots and Systems*, pp. 120–126, 1995, Pittsburgh, PA.

[30] B. Chen and J. K. Tugnait, "Multisensor tracking of a maneuvering target in clutter using IMMPDA fixed-lag smoothing," *IEEE Transactions on Aerospace and Electronic Systems*, vol. 36, pp. 983–991, 2000.

[31] Y. M. Chen and H. C. Huang, "Fuzzy logic approach to multisensor data association," *Mathematics and Computers in Simulation*, vol. 52, pp. 399–412, 2000.

[32] E. Cheung and V. J. Lumelsky, "Proximity sensing in robot manipulator motion planning: system and implementation issues," *IEEE Transactions on Robotics and Automation*, vol. 5, no. 6, pp. 740–751, December 1989.

[33] V. J. Lumelsky and E. Cheung, "Real-time collision avoidance in teleoperated whole-sensitive robot arm manipulators," *IEEE Transactions on Systems Man and Cybernetics*, vol. 23, no. 1, pp. 194–203, January/February 1993.

[34] P. M. Novotny and N. J. Ferrier, "Using infrared sensors and the Phong illumination model to measure distances," in *Proceedings of IEEE International Conference on Robotics and Automation*, pp. 1644–1649, Detroit, MI, 10–15 May 1999.

[35] B. T. Phong, "Illumination for computer generated pictures," *Communications of the ACM*, vol. 18, no. 6, pp. 311–317, June 1975.

[36] B. Andò and S. Graziani, "A new IR displacement system based on noise added theory," *Proceedings of the 18th IEEE Instrumentation and Measurement Technology Conference*, pp. 482–485, Budapest, Hungary, 2001.

[37] L. Korba, S. Elgazzar, and T. Welch, "Active infrared sensors for mobile robots," *IEEE Transactions on Instrumentation and Measurement*, vol. 43, pp. 283–287, 1994.

[38] K. Hashimoto, T. Tsuruta, K. Morinaka, and N. Yoshiike, "High performance human information sensor," *Sensors and Actuators A—Physical*, vol. 79, no. 1, pp. 46–52, 25 January 2000.

[39] N. Yoshiike, K. Morinaka, K. Hashimoto, M. Kawaguri, and S. Tanaka, "360 degrees direction type human information sensor," *Sensors and Actuators A—Physical*, vol. 77, pp. 199–208, 1999.

[40] P. J. de Groot, G. J. Postma, W. J. Melssen, and L. M. C. Buydens, "Validation of remote, on-line, near-infrared measurements for the classification of demolition waste," *Analytica Chimica Acta*, vol. 453, no. 1, pp. 117–124, 18 February 2002.

[41] D. M. Scott, "A 2-color near-infrared sensor for sorting recycled plastic waste," *Measurement Science and Technology*, vol. 6, no. 2, pp. 156–159, February 1995.

[42] Matrix Elektronik, AG, Kirchweg 24 CH-5422 Oberehrendingen, Switzerland, *IRS-U-4A Proximity Switch Datasheet*, 1995.

[43] M. D. Adams, "Lidar design, use, and calibration concepts for correct environmental detection," *IEEE Transactions on Robotics and Automation*, vol. 16, pp. 753–761, December 2000.

[44] X. D. He, K. E. Torrance, F. X. Sillion, and D. P. Greenberg, "A Comprehensive Physical Model for Light Reflection," *Computer Graphics*, vol. 25, no. 4, pp. 175–186, July 1991.

[45] E. R. Davies, *Machine Vision: Theory, Algorithms, Practicalites*, London: Academic Pr., 1990, pp. 377–382.

[46] R. M. Haralick and L. G. Shapiro, *Computer and Robot Vision*, Reading, Massachusetts: Addison-Wesley, vol. 2, 1993, pp. 1–11.

[47] A. Foessel–Bunting, "Radar sensor model for three-dimensional map building," *Proceedings SPIE, Mobile Robots XV and Telemanipulator and Telepresence Technologies VII*, vol. 4195, November 2000.

[48] Arrick Robotics, P.O. Box 1574, Hurst, Texas, 76053, URL: www.robotics.com/rt12.html, *RT-12 Rotary Positioning Table*, 2002.

[49] J. W. Goodman, *Introduction to Fourier Optics*, New York: McGraw-Hill, 2nd ed., 1996, pp. 246–249.

[50] B. Barshan and T. Aytaç, "Position-invariant surface recognition and localization using infrared sensors," submitted to *Optics Communications*, July 2002.

[51] T. Aytaç and B. Barshan, "Differentiation and localization of targets using infrared sensors," *Optics Communications*, vol. 210, no. 1–2, pp. 25–35, September 2002.